Chapter 6
Experimental and Numerical Investigation of Mass Transport in Porous Media

6.1 Measurement of Molecular Diffusion Coefficients

Mass transfer is a topic of central importance in chemical engineering, and molecular diffusion is the basic physical mechanism underlying mass transfer processes, even when convection comes into play. As a result, values of the molecular diffusion coefficient (D_m) are required for mass transfer calculations and extensive tabulations of this parameter have been prepared in the past (see [38, 41]). Equations for the prediction of D_m are also available and, in general, they have reasonable accuracy [44]. Nevertheless, it is important to determine values D_m experimentally, in many instances.

In the simple experiment described here, consideration is given to the process of mass transfer from a volatile solid sphere (a moth ball), buried in a packed bed of inert particles (sand or glass ballotini), through which air is forced to flow continuously. And also, to the similar process of dissolution of slightly soluble spheres buried in a packed beds of inerts through which water flows. These are important "model situations" for the understanding of such processes as char combustion in fluidised beds [42] and leaching of ore (or contaminant) from buried rocks (or buried waste).

When these processes are performed with very low fluid velocities, the rates of mass transfer are strongly determined by molecular diffusion and the experiment may be used to provide an accurate method for the measurement of the diffusion coefficient. It is an entirely novel method that has the added interest of easily providing data at temperatures and pressures that differ significantly from ambient values. This is not always easy to achieve with other methods [35].

As an introduction to the present analysis, it is useful to consider the simple situation depicted in Fig. 6.1a, where the vapour liberated by a buried sphere travels through the interstices of a packed bed of inerts, as a result of molecular diffusion.

F. A. Coutelieris and J. M. P. Q. Delgado, *Transport Processes in Porous Media*, Advanced Structured Materials 20, DOI: 10.1007/978-3-642-27910-2_6,

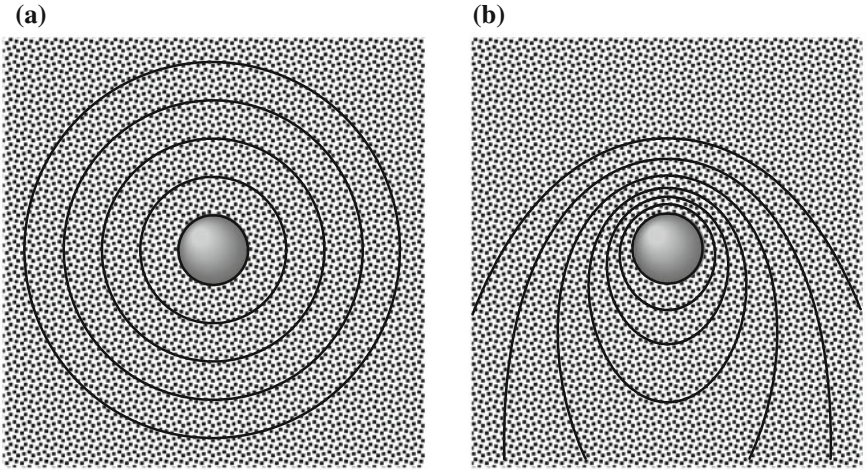

Fig. 6.1 Sketch of iso-concentration surfaces around active sphere of radius b for **a** pure diffusion, and **b** diffusion with convection

6.1.1 Diffusion Alone

The sphere of slightly volatile solid is assumed to be buried in a packed bed of sand, of "infinite extent", the interstices of the bed being filled with a stagnant gas (e.g. air) that is assumed to be free of solute at a large distance from the sphere (*i.e.* $C \to 0$ as $r \to \infty$). At $r = b$, where the active sphere contacts the gas phase, the molar concentration of solute in the gas is $C^* = P_V/RT$, where P_V is the equilibrium vapour pressure of the solute at the temperature (T) of the experiment.

The concentration gradient will give rise to a process of outwards diffusion of solute, but if diffusion is slow, the size of the sphere is taken to be constant, during one experiment; in other words, the assumption of a quasi-steady state is legitimate.

Under that assumption, the rate of diffusion across a spherical surface of radius r, concentric with the solid sphere, will be independent of r. From Fick's law,

$$n = -D'_m\left(4\pi r^2 \varepsilon\right)\frac{dC}{dr} \tag{6.1}$$

where $D'_m = D_m/\tau$ is the effective diffusion coefficient (τ being the tortuosity factor, accepted to be $\sqrt{2}$ for packed beds of granular materials [48] and ε is the bed voidage (assumed constant throughout). Since n is independent of r, integration of Eq. 6.1, between the limits $(r = b, C = C^*)$ and $(r \to \infty,\ C \to 0)$, gives

$$n = 4D'_m \varepsilon\, \pi\, b\,(C^* - 0) = 2\frac{D'_m}{d_1}\varepsilon\, \pi\, d_1^2\,(C^* - 0) \tag{6.2}$$

where $d_1\ (= 2b)$ is the diameter of the active sphere. Identifying (πd_1^2) as the area of the active sphere, helps recognize the expression for the mass transfer

coefficient as $k = 2\varepsilon D'_m/d_1$. Introduction of the Sherwood number, $Sh' = kd_1/D'_m$, shows that for mass transfer by pure diffusion, around a buried sphere,

$$\frac{Sh'}{\varepsilon} = 2 \tag{6.3}$$

an expression similar to the well known result, $Sh = 2$, for pure diffusion around a sphere in an unbounded fluid [48].

6.1.2 Diffusion with Convection

Figure 6.1b represents again the buried sphere, but now exposed to a constant flow of gas, with average interstitial velocity u_0. The solute still diffuses away from the surface of the sphere, but the rate of mass transfer is now enhanced, since the solute is continuously swept away by the moving fluid. The surfaces of equal concentration are no longer spheres. The analysis of the physical situation is complicated, but it has been worked out in detail [23]. For the conditions of interest in the present work, the expression

$$\frac{Sh'}{\varepsilon} = \left[4 + \frac{4}{5}\left(Pe'_p \frac{d_1}{d}\right)^{2/3} + \frac{4}{\pi}\left(Pe'_p \frac{d_1}{d}\right)\right]^{1/2} \tag{6.4}$$

has been shown to give accurate values of Sh'/ε, where $Pe'_p = u_0 d/D'_m$ is the Peclet number based on the diameter of the inert particles (d) making up the bed. It may be easily seen that Eq. 6.4 reduces to Eq. 6.3, in the limit of low Pe' ($= Pe'_p\, d_1/d$). As Pe'_p is increased, it is known that Eq. 6.4 becomes inaccurate [23]. At $Pe'_p \cong 1$, Eq. 6.4 is found to be accurate to within 5%, and therefore this value of Pe'_p should not be exceeded. This is because convective dispersion (rather than molecular diffusion) would then become the relevant mechanism of mass transfer in the packed bed. However, in the case of the experiments described below, conditions are strictly restricted to the range of applicability of Eq. 6.4.

The essence of the experimental method proposed relies on burying a weighed sphere of naphthalene (with initial mass m_0 and diameter d_1) in a packed bed of sand of known porosity (ε) and continuously forcing a metered stream of air (volumetric flowrate, v) through the packed bed (cross sectional area, A) for a given time interval, Δt. Weighing the sphere at the end of the time interval (mass m_t) gives the rate of sublimation as $(m_0 - m_t)/\Delta t$ and the mass transfer coefficient may be calculated from

$$k = \frac{m_0 - m_t}{\Delta t\, M\, \pi d_1^2\, (p_V/RT)} \tag{6.5}$$

where M is the molecular weight of naphthalene.

With the interstitial velocity given by $u_0 = v/(A\varepsilon)$, the only unknown in Eq. 6.4 is D'_m. A simple way of solving this equation relies on re-arranging it, through multiplication by D'_m $(= D_m/\sqrt{2})$, to obtain

$$\frac{kd_1}{\varepsilon} = D'_m \left[4 + \frac{4}{5} \left(\frac{u_0 d_1}{D'_m} \right)^{2/3} + \frac{4}{\pi} \left(\frac{u_0 d_1}{D'_m} \right) \right]^{1/2} \tag{6.6}$$

Several models can be found in the literature for the prediction of diffusion coefficients in binary systems [48]. Fuller et al. [21] suggest the use of the following equation

$$D_m = \frac{\left(\frac{M_A + M_B}{M_A M_B} \right)^{1/2} T^{1.75}}{P \left[(\Sigma v)_A^{1/3} + (\Sigma v)_B^{1/3} \right]^2} \times 10^{-7} \tag{6.7}$$

where P is the absolute pressure (in bar), M_A and M_B are, respectively, the molecular weights of components A and B (in g/mol), and $(\Sigma v)_A$ and $(\Sigma v)_B$ are the values of the atomic diffusion volumes of components A and B, which are tabulated in Reid et al. [44].

Equation 6.7 predicts a proportionality between D_m and $T^{1.75}/P$, and this is an important result that may be demonstrated using the experimental technique described in the following section.

6.1.3 Experiments

An example of the experimental setup is sketched in Fig. 6.2. The air supply may determine the maximum pressure at which the experiment can be performed. The tubing and valves connecting the air supply to the low pressure end of the rig will be standard material, for the maximum working pressure intended. The test column, containing the packed bed of sieved sand (or glass ballotini) may be made from a short piece of stainless steel tube (typically 80 mm internal diameter and 110 mm long) flanged at both ends. The test column is best kept vertical, to avoid settling of the packing to one side, and a downward gas flow will prevent unwanted fluidization of the bed material. A piece of some sort of gauze should be placed over the bottom plate of the test column to prevent the granular material from going into the tubing.

If the rotameter gives the flowrate v_R, at pressure P_R and temperature T_R, the actual flowrate in the test column is given as $v = v_R(P_R/P)(T/T_R)$, where P is the absolute pressure indicated in the manometer connected to the test column. The vapour pressure is calculated using Uno's correlation [53].

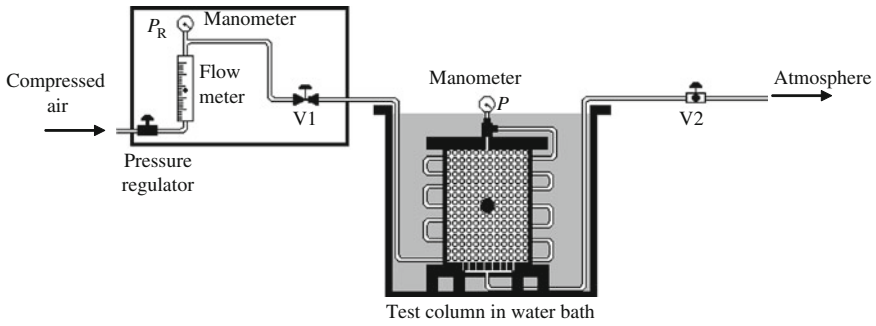

Fig. 6.2 Experimental set-up

In experiments at temperatures differing from ambient, the test column and a significant length of the tubing feeding it have to be kept in a constant temperature bath.

The naphthalene spheres used in the experiments were solidified from the melt, in simple moulds made of silicone rubber for the purpose. The diameter of each sphere was measured with callipers (along three perpendicular directions, to ensure near sphericity) and it was typically about 20 or 25 mm.

Each sphere was weighed accurately (initial mass, m_0), in an analytical balance, before burying it (with some care, to avoid unwanted erosion) near the middle of the packed bed, which had been previously immersed in the constant temperature bath for a long enough period of time. The top plate of the test column was then bolted in place and the column was tapped gently, a few times, to ensure close packing of the granular material. The test column and associated tubing were then immersed again in the constant temperature bath and the air supply was then connected, to give the intended test pressure and gas flowrate. The air flowrate was kept constant for a time Δt, following which it was interrupted and the test column was opened, to remove the sphere for weighing (final mass, m_t).

Each experiment lasted between 50 min and 60 h, the time being chosen to give a measurable loss of weight (typically, 0.05 g), that nevertheless would not correspond to a significant variation in the diameter of the sphere. The time intervals were however sufficiently long to reduce inaccuracies due to evaporation in the stages of sphere introduction and removal from the test column.

The experimental measurements of mass transfer in water were performed on the dissolution of individual spheres of for example, 2-napthol or benzoic acid, buried in beds of sand through which a metered stream of distilled water (which had been previously deaerated under vacuum) was forced to flow steadily.

Instead of weighing the sphere, the concentration of solute in the outlet stream, C_{out}, was continuously measured to give the rate of dissolution. C_{out} was measured by means of a UV/VIS spectrophotometer. When steady state was reached, the rate of dissolution of the solid could be found directly from $n = QC_{\text{out}}$, where Q is the measured volumetric flow rate of water.

6.2 Measurement of Dispersion Coefficients (Axial and Radial)

6.2.1 Measurement of Axial Dispersion Coefficients

Since the development of the dispersion approximation for the study of solute transport in capillary tubes by Taylor [52], the flow of the tracer is described by dispersion due to molecular diffusion and radial velocity variations. In packed beds, with $D/d > 15$, the assumption of flat velocity profiles and porosity is reasonable as point out by Akehata and Sato [1] and Gunn [25] and later showed by the experimental studies of Stephenson and Stewart [50] and Gunn and Pryce [26], that suggested $D/d > 10$.

Imagine a packed bed of uniform porosity (ε), contained in a long column of length L along which liquid flows at a superficial velocity U (the interstitial velocity is then $u = U/\varepsilon$) and initial concentration of solute C_0, in which a tracer with continuously injection and concentration of soluteC_S, is dispersed in radial and axial direction. Taking a small control volume inside this boundary layer, a material balance on the solute, with length dz and width dr, leads to (see [25])

$$D_L \frac{\partial^2 C}{\partial z^2} + \frac{1}{r}\frac{\partial}{\partial r}\left(D_T r \frac{\partial C}{\partial r}\right) - u\frac{\partial C}{\partial z} = \frac{\partial C}{\partial t} \tag{6.8}$$

Klinkenberg et al. [33] and Bruinzeel et al. [9] show that radial dispersion can be neglected in comparison with axial dispersion for a small ratio of column diameter to length (D/L) and large fluid velocity. The partial differential equation describing tracer transport in the bed reduces then to

$$D_L \frac{\partial^2 C}{\partial z^2} - u\frac{\partial C}{\partial z} = \frac{\partial C}{\partial t} \tag{6.9}$$

where z measures length along the bed, and if L is sufficiently large (semi-infinite bed) the appropriate boundary conditions are

$$C = C_0 \qquad 0 \le z \le L \qquad t = 0 \tag{6.10a}$$

$$uC_S = uC - D_L \frac{\partial C}{\partial z} \qquad z = 0 \qquad t > 0 \tag{6.10b}$$

$$\frac{\partial C}{\partial z} = 0 \qquad z = L \qquad t > 0 \tag{6.10c}$$

For a step input, the concentration at the outlet of the bed $(z = L)$ can be obtained by Carslaw and Jaeger [10], who give the exact solution of the equivalent heat transfer problem. However, a study developed by Harrison et al. [29] showed that the boundary conditions developed by Danckwerts [15], for an infinite system, hold adequately for a finite system provided $uL/D_L \ge 10$, So, for a step input

(from C_0 to C_S), the concentration at the outlet of the bed ($z = L$) is known [15] to be given, if L is sufficiently large, by

$$F(\theta) = \frac{1}{2}\left[1 - \text{erf}\left(\sqrt{\frac{LPe_L}{\theta d}}\frac{(1-\theta)}{2}\right)\right] \tag{6.11}$$

or for a pulse response by

$$E(\theta) = \frac{1}{2}\left(\frac{LPe_L}{\pi\theta d}\right)^{1/2} \times \exp\left[\frac{-LPe_L(1-\theta)^2}{4\theta d}\right] \tag{6.12}$$

Rifai et al. [45] and Ogata and Banks [39] showed that the solution of Eq. 6.9 with the boundary conditions and initial condition given by Eqs. 6.10a–c is

$$\begin{aligned} F(\theta) = &\frac{1}{2}\left[1 - \text{erf}\left(\sqrt{\frac{LPe_L}{\theta d}}\frac{(1-\theta)}{2}\right)\right] \\ &+ \frac{1}{2}\left[1 - \text{erf}\left(\sqrt{\frac{LPe_L}{\theta d}}\frac{(1+\theta)}{2}\right)\right]\exp\left(\frac{L}{d}Pe_L\right) \end{aligned} \tag{6.13}$$

However, Ogata and Banks [39] showed that for large molecular Peclet numbers (say, $uL/D_L > 100$), the advection dominates and the second term in the right-hand side can be neglected, with an error lesser than 5%, and Eq. 6.13 reduces to Eq. 6.11.

6.2.1.1 Experiments

Typically, dispersion along the direction of flow is studied by following the distortion of some concentration wave (of a tracer), as it progresses along the packing. In our experiments, a step in tracer concentration was introduced at the top of a long packed bed, of constant cross section, and the variation of tracer concentration, continuously in the stream leaving the bed, was recorded.

The partial differential equation describing tracer transport in the bed is given by Eq. 6.9 and for a step input (from C_0 to C_S), the concentration at the outlet of the bed ($z = L$) is known [15] to be given by

$$\frac{C - C_0}{C_S - C_0} = \frac{1}{2}\left[1 - \text{erf}\left(\frac{L - ut}{2\sqrt{D_L t}}\right)\right] \tag{6.14}$$

if L is sufficiently large. This result may be written as Eq. 6.11, where $F = (C - C_0)/(C_S - C_0)$ is the dimensionless concentration rise and $\boldsymbol{\theta} = t/\bar{t}$ is the dimensionless time ($\bar{t}$ being the mean residence time of fluid in the bed).

For each set of C *vs.* t values, obtained in one experiment, the values of F *vs.* θ were calculated and the value of Pe_L determined to give the least deviation

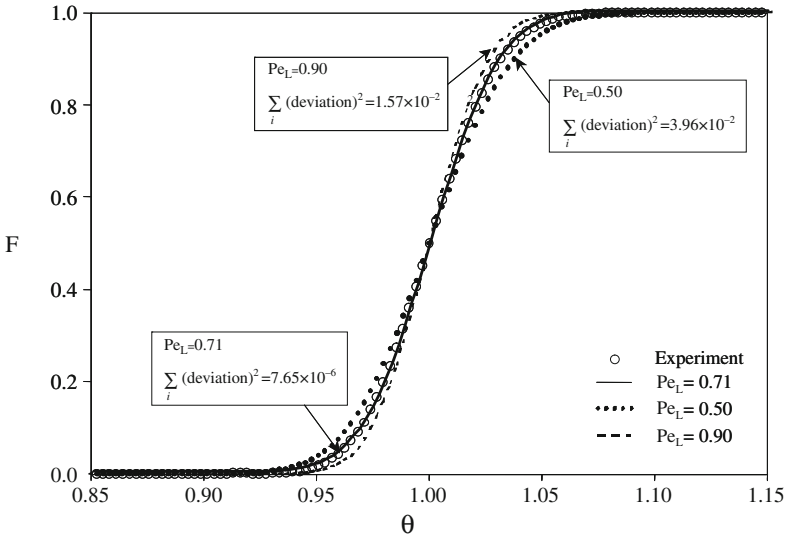

Fig. 6.3 Comparison of experiment with Eq. 6.4 for three values of Pe_L

between the experimental points and the line representing Eq. 6.11. Figure 6.3 helps illustrate the method and it also gives some idea about its sensitivity to variations inPe_L.

The rig used in the majority of our experiments (including all those at temperature above ambient) is sketched in Fig. 6.4, but the various items are not to scale. Two large stainless steel reservoirs (about 0.3 m in diameter and 1.0 m tall) were used to keep the distilled water and the dilute solution of sodium chloride (up to 1.5 kg/m^3 in salt) immersed in a silicone oil thermostatic bath. The use of very dilute salt solutions and the care taken in equalizing the temperature of both liquids is needed to avoid dispersion by natural convection. Both the distilled water and the salt solution were degassed "in situ", by bubbling under vacuum, to avoid liberation of small air bubbles inside the test column, at the higher temperatures. Both reservoirs were connected (at the top) to the compressed air line (approx.: 4 bar) to have the rig permanently pressurised and help discharge the liquid through the flow regulating valve V, open to the atmosphere.

At the top of the test column (3.0 m long and 0.047 m in diameter, made of brass), a three-way valve (T) could be manipulated to select the feed. At the beginning of each experiment it was turned to let distilled water flow through the bed, until no salt was detected in the conductivity meter monitoring the exit stream. After that, it was turned to allow the salt solution to go through the column, at a constant flowrate, measured by an orifice meter connected to a differential pressure transducer. The dead space between the three-way valve and the top of the bed was less than 0.1% of the void space in the bed proper and this is important to ensure that a sharp step input of tracer is obtained in the bed. The conductivity

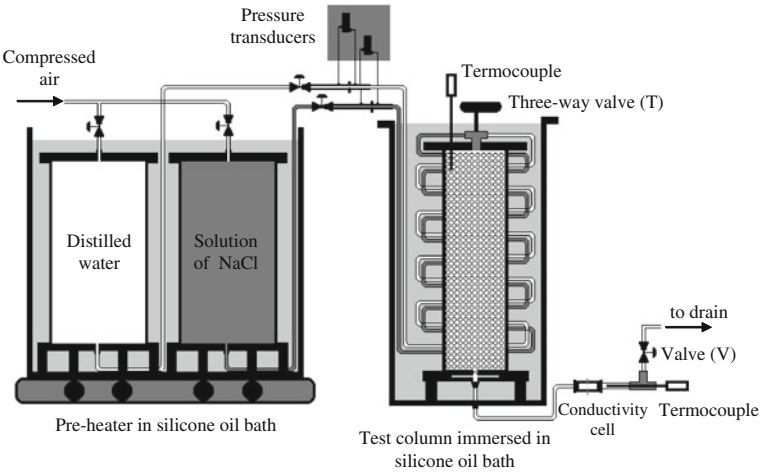

Fig. 6.4 Diagram of experimental set-up

cell at the exit of the test column was connected to a micro-computer and values of the salt concentration were recorded at a frequency of 10 Hz. Care was taken to have a negligible volume of liquid between the bottom of the bed and the conductivity cell in order to avoid distortion of the signal read by the cell. A typical record of outlet tracer concentration is shown in Fig. 6.3 and from the sensitivity of the curves representing Eq. 6.11, to the value of Pe_L, it may be guessed that the values of D_L obtained are accurate to within $\pm 15\%$.

6.2.2 Measurement of Radial Dispersion Coefficients

The radial dispersion coefficient can be determined by plotting ($\%$ composition : C_{10} and C_{90}) *vs* (distance from 50% composition) on arithmetic-probability paper [40]. The dispersion coefficient can be calculated by

$$D_T = \frac{u}{L}\left(\frac{C_{90} - C_{10}}{3.625}\right)^2 \tag{6.15}$$

The most widely used techniques for the measurement of lateral dispersion are the continuous point source and the instantaneous finite source methods (see *e.g.* [46]), which rely on the injection of tracer in a flowing liquid, followed by tracer detection at several points, downstream of the injection point. If at time $t = 0$ a tracer is injected into the porous medium from an injector, for the continuous point source method the tip of the injector is taken as the tracer origin. For the instantaneous finite source method the origin lays just down-gradient of the tracer injector.

Several authors like Roemer et al. [47] and Gunn and Pryce [26] used the solution of Eq. 6.15 when the axial dispersion coefficient is taken equal to radial dispersion coefficient. However, in this work we only consider experimental techniques where axial dispersion is neglected.

6.2.2.1 "Instantaneous Finite Source" Method

The method adopted by some authors like Dorweiler and Fahien [16] and Fahien and Smith [19] is based that the tracer is fed into the main stream at a point on the axis on the column.

The analytical model for an instantaneous finite source in one dimension is first presented by Crank [13]. Baetsle [6] extended the model to three-dimensional dispersion. Hunt [32] and Sun [51] provided the three-dimensional solution to the advection–dispersion equation [6] using different mathematical analysis. Van Genuchten and Alves [54] presented a number of analytical solutions of the one-dimensional convective–dispersive solute transport equation.

Tracer concentration should be low enough to avoid density-induced flow effects. The tracer should be conserved (*i.e.* not destroyed) in the experiment and the distribution of flow rates at the outlet must be the same as in the feed so as not to induce complications in the flow field.

Radial dispersion may be evaluated by injecting a steady flow of a tracer at a point of a test section column. For a boundary layer, which is thin in comparison with the length of the axial distance (L), axial dispersion will be negligible. Taking a radial co-ordinate, r, to measure distance to the axis of the bed and a co-ordinate z, to measure distance along the average flow direction, the differential mass balance on the solute reads

$$\frac{D_T}{r}\frac{\partial}{\partial r}\left(r\frac{\partial C}{\partial r}\right) = u\frac{\partial C}{\partial Z} \tag{6.16}$$

where D_T is the radial dispersion coefficient. Fahien and Smith [19] solved the differential dispersion Eq. 6.16 with

$$z = 0 \quad 0 < r < R_i \quad C = C_0 \tag{6.17a}$$

$$z = 0 \quad R_i < r < R \quad C = 0 \tag{6.17b}$$

$$\text{all } z \quad r = R;\ r = R_i \quad \frac{\partial C}{\partial r} = 0 \tag{6.17c}$$

and the solution of Eq. 6.16 with the boundary conditions (6.17a–c) is

$$\frac{C}{C_0} = 1 + \frac{2R}{R_i}\sum_{n=1}^{\infty}\frac{J_1(\beta_n R_i/R)J_0(\beta_n r/R)}{\beta_n J_0^2(\beta_n)}\frac{z}{R}\exp\left[-\frac{\beta_n^2}{Pe_T}\frac{z}{R}\right] \tag{6.18}$$

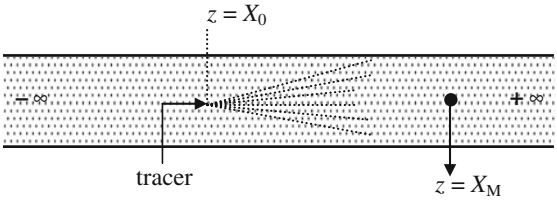

Fig. 6.5 A schematical diagram of test section for radial dispersion

where J_0 and J_1 are the Bessel functions of the first kind, of order 0 and 1, respectively, and the β_n are the positive roots of the Bessel function of the first kind, of order 1.

6.2.2.2 "Continuous Point Source" Method

This method is based on the measurement of radial mass exchange between two coaxial portions of a packed bed, along which liquid flows, parallel to the axis; the feed to the central portion is water containing a small amount of sodium chloride and that to the outer portion is pure water.

Klinkenberg et al. [33] derived an analytical solution for Eq. 6.16, neglecting the effect of injector radius (see Fig. 6.5), with the boundary conditions given by

$$z = +\infty \quad \text{all } R \quad C = C_0 \tag{6.19a}$$

$$z = -\infty \quad \text{all } R \quad C = 0 \tag{6.19b}$$

$$\text{all } z \quad r = R;\ r = 0 \quad \frac{\partial C}{\partial r} = 0 \tag{6.19c}$$

and the solution of Eq. 6.16 with the boundary conditions (6.19a–6.19c) is

$$\frac{C}{C_0} = 1 + \sum_{n=1}^{\infty} \frac{J_0(\beta_n r/R)}{J_0^2(\beta_n)} \exp\left[-\frac{\beta_n^2 D_T z}{R^2 u}\right] \tag{6.20}$$

where J_0 is the Bessel function of the first kind, of order 0, and the β_n are the positive roots of the Bessel function of the first kind, of order 1.

Plautz and Johnstone [43] and Sinclair and Potter [49] used Eq. 6.9 for an infinite case, where no boundary is present, of mass diffusion from a point source. The result with axial dispersion neglected was given by Carslaw and Jaeger [10]

$$\frac{C}{C_0} = \frac{R^2 u}{4 D_T z} \exp\left(-\frac{r^2 u}{4 D_T z}\right) \tag{6.21}$$

This solution includes a simplification possible when $z/r > 5$ (axial dispersion neglected).

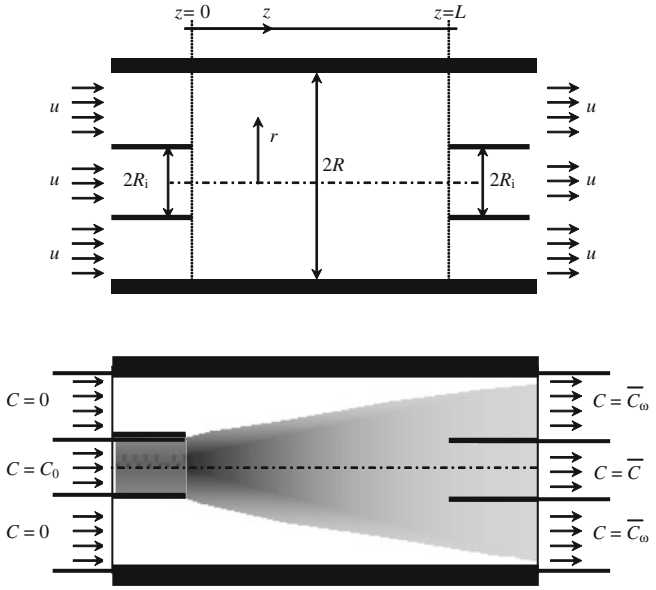

Fig. 6.6 Sketch of boundary conditions proposed by [30]

Blackwell [8] assumes the effect of radius injector and gives the analytical solution to the differential equation describing radial dispersion in the absence of axial dispersion. Hiby and Schummer [30] presented a solution of Eq. 6.16 that considered the tracer pipe to be of significant diameter compared to the diameter of the bed (see Fig. 6.6), and the boundary conditions adopted were

$$\mathrm{z} > 0 \quad r = R \quad \frac{\partial C}{\partial r} = 0 \tag{6.22a}$$

$$\mathrm{z} = 0 \quad r < R_\mathrm{i} \quad C = C_0 \tag{6.22b}$$

$$\mathrm{z} = 0 \quad R_\mathrm{i} < r < R \quad C = 0 \tag{6.22c}$$

On the assumption that D_T and u are independent of position, the solution of Eq. 6.9 following Hiby and Schummer [30] gives, for the resulting outlet average concentration in the inner stream of liquid,

$$\frac{\overline{C}}{C_0} = 4 \sum_{\mathrm{n}=0}^{\infty} \frac{\mathrm{J}_1^2(\beta_\mathrm{n} R_\mathrm{i}/R)}{\beta_\mathrm{n}^2 \mathrm{J}_0^2(\beta_\mathrm{n})} \exp\left[-\frac{Ld}{\mathrm{Pe_T}} \left(\frac{\beta_\mathrm{n}}{R} \right)^2 \right] \tag{6.23}$$

where J_0 and J_1 are the Bessel function of the first kind, of orders 0 and 1, respectively, and the β_n are the positive roots of the Bessel functions of the first kind, of order 1. The measurement of $\bar{C}$ and C_0 provides a method for the determination of $\mathrm{Pe_T}$ (and therefore of D_T), since all other parameters in the equation are known.

Harleman and Rumer [28] and Han et al. [27] consider a steady-state experiment in a rectangular column. The authors solved the differential equation with the boundary conditions,

$$C = C_0 \quad x = 0 \quad 0 < y < +\infty \tag{6.24a}$$

$$C = 0 \quad x = 0 \quad -\infty < y < 0 \tag{6.24b}$$

$$\frac{\partial C}{\partial y} = 0 \quad \text{all } x \quad y \to \pm\infty \tag{6.24c}$$

and the solution obtained for a step input in concentration, is

$$\frac{C}{C_0} = \frac{1}{2}\left[1 - \text{erf}\left(\sqrt{\frac{\text{Pe}_\text{T}}{Ld}}\frac{y}{2}\right)\right] \tag{6.25}$$

6.2.2.3 Mass Transfer From a Flat Surface Aligned With the Flow

Coelho and Guedes de Carvalho [12] developed a new experimental technique, based on the measurement of the rate of dissolution of planar or cylindrical surfaces, buried in the bed of inert particles and aligned with the flow direction.

Figure 6.7a sketches a section through a packed bed along which liquid is flowing, close to a flat wall, part of which ($0 < x < L$) is slightly soluble. Liquid flow will be taken to be steady, with uniform average interstitial velocity u, and if the concentration of solute in the liquid fed to the bed is C_0 and the solubility of the solid in the wall is C^*, a mass transfer boundary layer will develop, across which the solute concentration drops from $C = C^*$, at $y = 0$, to $C \to C_0$, for large y.

The question of how large is meant by a "large y" needs some clarification. Obviously, if L were only of the order of a few particle diameters, and u were large, the concentration of solute would fall to C_0 over a distance of less than one particle diameter. In that case, flow in the bulk of the packed bed would have little influence on the mass transfer process, which would be dominated by diffusion in a thin layer of liquid, adjacent to the soluble surface. Already for large L and low u, the thickness of the mass transfer boundary layer will grow from zero, at $x = 0$, to a value of several particle diameters, at $x = L$ and the process of mass transfer will then be determined by a competition between advection and dispersion in the bulk of the bed. Now, it is well known (*e.g.* [55]) that the voidage of a packed bed (and therefore the fluid velocity) is higher near a containing flat wall, but in the case of Guedes de Carvalho and Delgado [24] experiments it may be considered that such a non-uniformity will have negligible effect. For one thing, we work with bed particles of between 0.2 and 0.5 mm and therefore the region of increased voidage will be very thin. Furthermore, because the inert particles making up the bed indent the soluble surface slightly, as dissolution takes place (and this slight indentation is easily confirmed when the piece of soluble solid is removed from

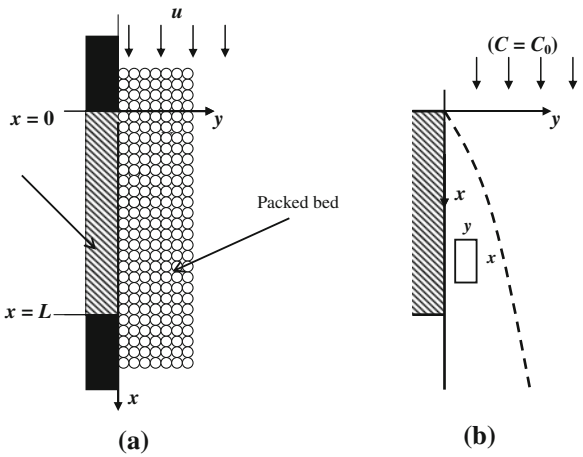

Fig. 6.7 **a** Flow along soluble slab, **b** Mass transfer boundary layer

within the bed), there is in fact virtually no near wall region of higher voidage. Confirmation of these assumptions is given by the results of the experiments described below.

Taking a small control volume inside this boundary layer (see Fig. 6.7b), with side lengths δx, δy and unity (perpendicular to the figure), it is possible to perform a mass balance on the solute, for the steady state. If the boundary layer is thin, compared to the length of the soluble slab, axial dispersion is likely to be negligible, since the surface $y = 0, 0 < x < L$, is a surface of constant concentration ($C = C^*$).

Noting that the surface $y = 0,\ 0 < x < L$, is a surface of constant concentration, along which $\partial^2 C/\partial x^2 = 0$ and axial dispersion will be negligible, for a boundary layer which is thin in comparison with the length of the soluble slab. (A conservative criterion for this approximation to be valid is $L/d > 20$). For a slab the equation of diffusion in one dimension is

$$u\frac{\partial C}{\partial x} = D_{\mathrm{T}}\frac{\partial^2 C}{\partial y^2} \tag{6.26}$$

to be solved with

$$C = C_0 \quad x = 0 \quad y > 0 \tag{6.27a}$$

$$C = C^* \quad x > 0 \quad y = 0 \tag{6.27b}$$

$$C \to C_0 \quad x > 0 \quad y \to \infty \tag{6.27c}$$

The solution is

$$\frac{C - C_0}{C^* - C_0} = \mathrm{erfc}\left(\frac{y}{2\sqrt{D_T x/u}}\right) \tag{6.28}$$

and the flux of dissolution at any point on the slab surface may be obtained from (6.28) as

$$N = -D_T \varepsilon \left(\frac{\partial C}{\partial y}\right)_{y=0} = (C^* - C_0)\varepsilon \left(\frac{D_T}{\pi x/u}\right)^{1/2} \tag{6.29}$$

The instant rate of solid dissolution over the whole slab surface may now be calculated by integration of the local flux; taking a width b along the surface of the solid, perpendicular to the flow direction, there results

$$n = \int_0^L N\, b\, dx = (C^* - C_0)\varepsilon\, b\, L \left(\frac{4D_\mathrm{T}}{\pi L/u}\right)^{1/2} \tag{6.30}$$

and it is useful to define the coefficient

$$k = \frac{n}{(bL)(C^* - C_0)} = \varepsilon \left(\frac{4D_\mathrm{T}}{\pi L/u}\right)^{1/2} \tag{6.31}$$

This result shows how the measurement of the rate of dissolution of the solid, which is directly related to the average mass transfer coefficient, may be used to determine the coefficient of radial dispersion in the bed.

A simple way of checking the result in Eq. 6.31 is afforded by the predicted proportionality between k and the inverse square root of L. Experiments performed by Coelho and Guedes de Carvalho [12] with a wide range of slab lengths, both for the dissolution of benzoic acid in water and the sublimation of naphthalene in air, confirm the general validity of the above theory, provided that the approximate criterion

$$\frac{L}{d} \geq 0.62 \left(\frac{ud}{D_m}\right) \tag{6.32}$$

is observed, where D_m is the molecular diffusion coefficient of the solute. When the above criterion is not observed, the near wall film resistance to diffusion will have to be taken into account and approximate ways of doing this are described by Coelho and Guedes de Carvalho [12].

The similarity between the result given by Eq. 6.32 and that obtained by Higbie [31], for gas–liquid mass transfer by surface renewal, is striking. Equation 6.24a–c simply states that the average mass transfer coefficient, for the soluble wall, is that corresponding to surface renewal with a time of contact $t_\mathrm{c} = L/u$ and an apparent diffusion coefficient D_T.

6.2.2.4 Mass Transfer From a Cylinder Aligned With the Flow

For practical reasons, it proves simpler to perform experiments in which the dissolving solid is a cylinder, aligned with the flow direction and it is important to know the theoretical expressions relating the average mass transfer coefficient with the coefficient of dispersion, D_T, for that situation.

Fortunately, under appropriate conditions, easy to reproduce in the laboratory, the thickness of the mass transfer boundary layer is small in comparison with the radius of the dissolving cylinder and under such circumstances, the analysis presented above, for dissolution from a flat surface, is still applicable with good accuracy.

However, there are instances in which this simplification is not valid and an exact solution may be worked out in cylindrical co-ordinates, as shown by Coelho and Guedes de Carvalho [12].

The resulting expression for k is cumbersome to evaluate, but for small values of the parameter $\theta_c = D_T t_c / a^2$, where $t_c = L/u$ is the time of contact between liquid and solid, a good approximation is

$$k = \varepsilon \left(\frac{4D_T}{\pi t_c} \right)^{1/2} \left(1 + \frac{\sqrt{\pi}}{4} \theta_c^{1/2} - \frac{1}{12} \theta_c + \frac{\sqrt{\pi}}{32} \theta_c^{3/2} - \cdots \right) \tag{6.33}$$

For higher values of θ_c, up to θ_c =0.4, the first four terms may be used, instead of the infinite series on the right hand side of Eq. 6.33, with an error of less than 1% in k.

6.2.2.5 Experiments

Experiments were performed on the dissolution of individual cylinders of 2-napthol, buried in beds of sand through which a metered stream of distilled water (which had been previously deaerated under vacuum) was forced to flow steadily, as sketched in Fig. 6.8. The beds of sand were contained in a stainless steel column 500 mm long and 100 mm in internal diameter, with the cylinder of 2-napthol placed co-axially inside it, all in vertical alignment. The cylinders of 2-napthol had a diameter of 20 mm and a length of 250 mm and they were tightly mounted in alignment between two rods of stainless steel (each 20 mm in diameter and 100 mm long). These two metal rods fulfilled the double purpose of covering the top and bottom of the 2-napthol cylinder and straightening the flow field, upstream and downstream from it; they also provided the points of support for alignment with the stainless steel column. Near the bottom of the stainless steel column, a perforated plate, covered with fine stainless steel wire mesh, was used to support the bed of sand and the cylinder inside it. The preparation and assemblage of the cylinders of 2-napthol followed closely the method detailed by Coelho and Guedes de Carvalho [12] for the preparation of cylinders of benzoic acid. The use of 2-napthol instead of benzoic acid was determined by the need to work at high temperatures and the relevant properties of 2-naphtol.

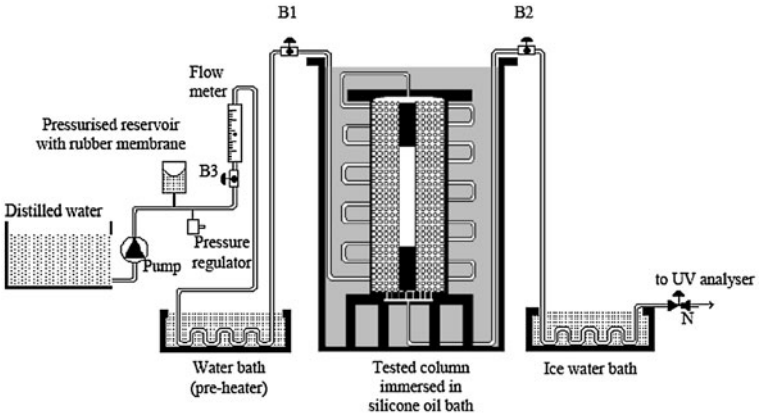

Fig. 6.8 Diagram of experimental set-up

Before any new series of runs, the cylinder buried in the sand (and when required, the sand itself) had to be replaced. In order to do that, ball valves B1 and B2 were closed and disconnected from the upstream and downstream piping, respectively, so as to allow the test column and the associated copper coil (and valves B1 and B2 in the ends) to be lifted from the thermostatic bath. Following that, the free ends of valves B1 and B2 were connected to plastic tubing that could be supplied with distilled water or directed to the drain. After removing the lid of the test column, distilled water was forced up through the bed of sand, so as to fluidise it slightly and allow the cylinder to be replaced without difficulty. As the water flow was stopped, to allow the sand particles to settle, the column was vibrated for a few seconds to give a good compaction of the bed. The lid of the test column was placed back in position and the stainless steel column (with attached copper coil and valves B1 and B2) was again immersed in the silicone oil bath. After connection to the main water circuit, valves B1, B2, and valve B3 were fully open and the flowrate of water fed to the top of the column was adjusted by means of valve N. The silicone oil bath was then heated to the required temperature of operation. A pre-heater helped warm up the water feed to near the temperature of the bath and an ice water bath was used to cool the liquid stream leaving the test column, before it passed the valve regulating the flow. In this way it was possible to perform experiments at temperatures up to the normal boiling point of water (and above it, if necessary).

The concentration of 2-naphtol in the outlet stream, C_{out}, was continuously measured by means of a UV/VIS Spectrophotometer, set at 274 nm, and when steady state was reached, the rate of dissolution of the solid could be found from $n = QC_{out}$, where Q is the measured volumetric flow rate of water.

For the second example, a rig was built as sketched in Fig. 6.9, that allowed experiments to be performed over a wide range of temperatures. Two large reservoirs, of about 0.06 m^3 internal volume, were used to store distilled water and a

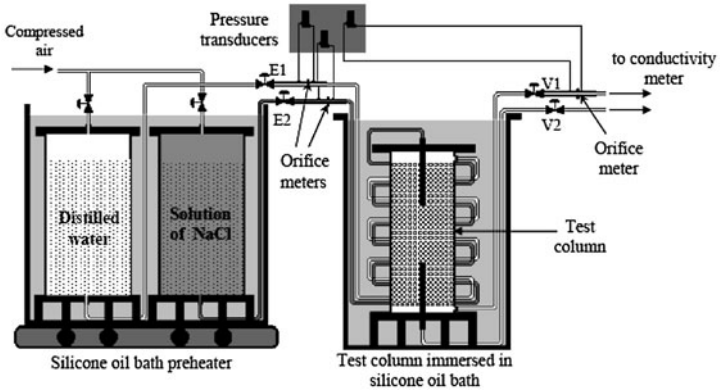

Fig. 6.9 Sketch of experimental set-up for measurement of radial dispersion coefficient

dilute solution of NaCl in distilled water with a concentration of salt of approximately 1.5 kg/m^3; both reservoirs were connected, at the top, to a source of air at 4 bar. The two reservoirs were kept in a thermostatic bath that was set at the temperature of the experiment, or at 353 K, when the experiments were performed above that temperature. The liquid held in each reservoir had been initially deaerated by stripping under vacuum, at room temperature, to avoid subsequent liberation of gas bubbles in the liquid streams going through the packed bed. In the test column, care was taken to have a good alignment of the axes of the inlet and outlet tubes of the core stream with that of the packed bed. The apparatus was kept in vertical alignment to avoid "settling" of the packing to any one side. Liquid flow was driven by the difference in pressure between the reservoirs and the exit sections, at atmospheric pressure. Valves V1 and V2 were used to adjust the outlet flowrate of each stream, to give equal velocity in the core tube and in the annulus, at the outlet; by acting slightly on valves E1 or E2 it was then possible to also impose equal velocities in the inlet streams to the bed. At the higher temperatures, the outlet streams had to be cooled before reaching valves V1 and V2, to avoid vaporization downstream of these valves, due to de-pressurization. The conductivity meter cell was built on a 30 mm nylon rod, 75 mm long, having a 10 mm hole drilled along its axis. Two platinum wires, 0.5 mm in diameter, crossed the wall of this nylon tube along opposite ends of one diameter of the mid cross section and they were glued in place, leaving a distance of about 8 mm between their tips. The platinum electrodes were connected to three 1 kΩ resistances (to within 0.01%) to form a Wheatstone bridge that was connected to a 9.30 V source, so that the liquid flowing through the cell acted as the variable resistance. The output of this conductivity meter was connected to a micro-computer and care was taken to calibrate the meter at the operating temperatures, whenever fresh solutions were introduced in the reservoirs. After allowing steady state to be reached, the rate of solute transfer from the core stream to the annulus is given simply as $n = v\left(C_0 - \overline{C}\right)$, where v is the volumetric flowrate of the core stream and $\overline{C}$ is the

average concentration of salt in that stream, at the exit. Care was taken to check that the value of n agreed with $n = \omega\,\overline{C}_{\omega}$, where ω is the volumetric flowrate of the stream going through the annulus and $\overline{C}_{\omega}$ the corresponding average salt concentration, at the outlet.

6.3 Measurement of Solubility at Different Temperatures

Solubility is perhaps the most fundamental of all chemical phenomena. The significance of what dissolves what, to what extent, at what temperature and pressure, and the effects of other species, was recognized at a very early stage. In more recent times the importance of solubility phenomena has been acknowledged throughout science. For example, in the environment, solubility phenomena influence the weathering of rocks, the creation of soils, the composition of natural water bodies and the behaviour and fate of many chemicals.

The characteristic ability of water to behave as a polar solvent changes when water is subjected to high temperatures and pressures. As water becomes hotter, its molecules seem much more likely to interact with non-polar molecules. For example, at 300°C (and high pressure) water has dissolving properties very similar to acetone, a common organic solvent.

Also, solid–liquid and solid–gas mass transfer investigations with Newtonian or non-Newtonian fluids are frequently made by following the rate of dissolution of a low solubility solute. In all researches, accurate solubility data are required.

On mass transfer investigations in porous media, as in studies of dispersion coefficients and solute transport, the most common solutes used are benzoic acid, 2-naphthol, naphthalene, salicylic acid and succinic acid with water or air (see [56]). In these experiments, knowledge of accurate solubility data at different temperatures is very important, *i.e.*, for low solubility solutes.

The experiment proposed is simple and inexpensive, and it provides an accurate method for the measurement of solubilities of solid solutes in liquids and gases. Consider a vertical column of length L, containing a packed bed of soluble spherical particles of diameter d_1. If liquid flow is steady, with a uniform volumetric flowrate Q, if the concentration of solute in the liquid fed to the bed is c_0 and the solubility of the solid particle is c^*, a mass transfer boundary layer will develop.

In the analysis of results of experiments of dissolution of soluble spherical particles in liquid flow, the equation for dissolution rate is given by,

$$Q\frac{\partial c}{\partial x} = kS_{\mathrm{L}}(c^* - c_0) \tag{6.34}$$

where S_{L} is the active surface area per unit length and k is the average mass transfer coefficient. Given constant flowrate, uniformly distributed particles and isothermal conditions, Eq. 6.34 is integrated between the inlet and outlet conditions of the bed, $x = 0$ to $x = L$ and $c = c_0$ to $c = c$. The following equation results,

$$\frac{c - c_0}{c^* - c_0} = 1 - \exp\left(-\frac{kS_L}{Q}L\right) \tag{6.35}$$

In order to guarantee that the outlet stream is saturated, it's important to observe the approximate criterion $(c - c_0)/(c^* - c_0) > 0.999$ (error less that 0.1%). The number of soluble spheres presented in a packed bed is given by,

$$n = \frac{V_{\text{colunn}}}{V_{\text{particle}}} = \frac{3}{2}\frac{(1-\varepsilon)D^2L}{d_1^3} \tag{6.36}$$

and the general validity of the above theory holds, provided that the approximate criterion

$$\frac{6(1-\varepsilon)kL}{u_0\varepsilon\, d_1} > 6.908 \tag{6.37}$$

If the criterion of Eq. 6.37 is to be satisfied, it is important to know the value of the average mass transfer coefficient, k, so as to be able to estimate the interstitial velocity of liquid, u_0.

6.3.1 Mass Transfer Around a Buried Soluble Sphere

For the propose of analysis, let as consider the situation of a slightly soluble sphere of diameter $d_1(=2a)$ buried in a bed of inert particles of diameter d (with $d \ll d_1$), packed uniformly (void fraction ε) around the spheres. The packed bed is assumed to be "infinite" in extent and a uniform interstitial velocity of liquid, u_0, is imposed, at a large distance from the spheres.

In order to obtain the flow field in the vicinity of the buried sphere, Darcy's law, $\mathrm{u} = -K\,\mathbf{grad}\,p$, is coupled with the continuity equation, $div\ \mathrm{u} = 0$, and Laplace's equation, $\nabla^2\phi = 0$, is obtained for the flow potential $\phi = k\,p$.

In terms of spherical coordinates (r, θ), the potential and stream functions are, respectively (see [14]),

$$\phi = -u_0\left[1 + \frac{1}{2}\left(\frac{a}{r}\right)^3\right] r\cos\theta \tag{6.38}$$

$$\psi = \frac{u_0}{2}\left[1 - \left(\frac{a}{r}\right)^3\right] r^2\sin^2\theta \tag{6.39}$$

and the velocity components are

$$u_r = \frac{\partial\phi}{\partial r} = -u_0\cos\theta\left[1 - \left(\frac{a}{r}\right)^3\right] \tag{6.40}$$

$$u_\theta = \frac{1}{r}\frac{\partial \phi}{\partial \theta} = u_0 \sin\theta \left[1 + \frac{1}{2}\left(\frac{a}{r}\right)^3\right] \tag{6.41}$$

Making use of the potential and stream lines, it is possible to perform a material balance on the solute in a differential element of a "stream tube" to obtain (see [11])

$$\frac{\partial c}{\partial \phi} = \frac{\partial}{\partial \phi}\left(D_L \frac{\partial c}{\partial \phi}\right) + \frac{\partial}{\partial \psi}\left(D_T \omega^2 \frac{\partial c}{\partial \psi}\right) \tag{6.42}$$

where ω is the distance to the flow axis, and D_L and D_T are the longitudinal and transverse dispersion coefficients, respectively.

The boundary conditions to be observed in the integration of Eq. 6.42 are: (1) the solute concentration is equal to the background concentration, c_0, far away from the sphere; (2) the solute concentration is equal to the equilibrium concentration, $c = c^*$, on the surface of the sphere and (3) the concentration field is symmetric about the flow axis.

For very low fluid velocities, dispersion is the direct result of molecular diffusion, with $D_T = D_L = D'_m$, and the numerical solution presented by Carvalho et al. [11] applies. Those authors suggest that their results are well approximated (with an error of less than 1%) by

$$k = \varepsilon \frac{D'_m}{d_1}\left[4 + \frac{4}{5}(\mathrm{Pe}')^{2/3} + \frac{4}{\pi}\mathrm{Pe}'\right]^{1/2} \tag{6.43}$$

where $\mathrm{Pe}' = u_0 d_1 / D'_m$ is the Peclet number for the soluble sphere.

Now, by substituting the average mass transfer coefficient, given by Eq. 6.43, into Eq. 6.37, the following expression is obtained for the approximate validity criterion of theory developed above:

$$\frac{1}{\mathrm{Pe}'}\left(1 + \frac{\pi}{\mathrm{Pe}'} + \frac{\pi}{5(\mathrm{Pe}')^{1/3}}\right) > \left(\frac{d_1}{(1-\varepsilon)L}\right)^2 \tag{6.44}$$

Finally, with Eq. 6.44 we could predict the volumetric flowrates that guarantee saturation in the outlet stream, $Q = \mathrm{Pe}'\pi D^2 \varepsilon D'_m/(4d_1)$. However, an important aspect to consider is the dependence of Q on the effective molecular diffusion coefficient, D'_m. Fortunately, values of D'_m increase with temperature, and the value of D'_m, at room temperature or lower, is a good estimate.

6.3.2 Experimental Set-Up

Experiments were performed on the dissolution of spheres of benzoic acid, 2-naphthol and salicylic acid (6.0 mm of internal diameter), buried in beds of sand

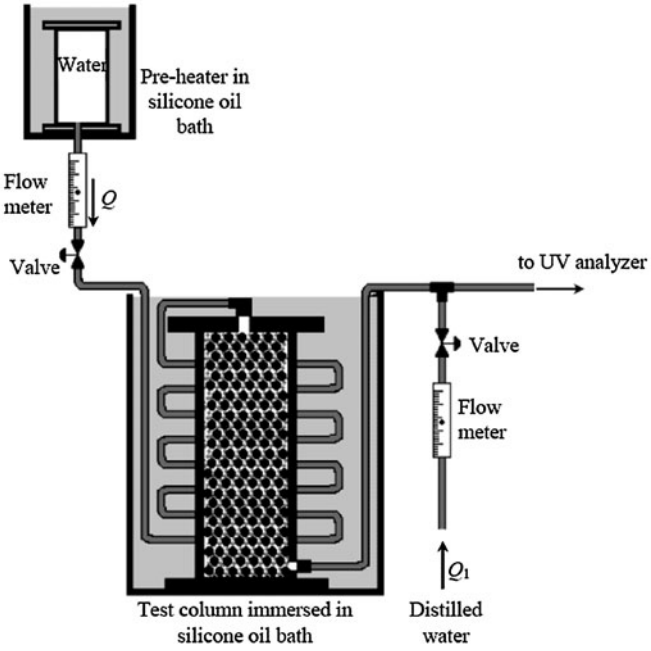

Fig. 6.10 Sketch of experimental set-up

(0.496 mm average particle diameter) through which water was steadily forced down, at temperatures in the range 293–373 K.

A stainless steel tube (21 mm i.d. and 200 mm long) was used to hold the bed of soluble solid spheres in an upright position while a metered stream of distilled water was fed to the top of the column, as sketched in Fig. 6.10. Near the bottom of the stainless steel column, a perforated plate, covered with fine wire mesh, was used to support the bed.

The distilled water was initially dearated, under vacuum, to avoid liberation of gas bubbles in the rig, at high temperature. The test column was immersed in a silicone oil bath kept at the desired operating temperature by means of a thermosetting bath head (not represented in Fig. 6.10). The copper tubing feeding the distilled water to the column at a constant metered rate was partly immersed in a pre-heater and it had a significant length immersed in the same thermosetting bath as the test column; the copper tubing leaving the test column was immersed in a chillier to cool the outlet stream before reaching the UV analyser.

The water flowrate was then adjusted to the required value, Q, and the concentration of solute in the outlet stream was continuously monitored by means of a UV/VIS Spectrophotometer (set at 274 nm, for 2-naphtol, at 226 nm, for benzoic acid and 292 nm, for salicylic acid).

The solubility of the solutes studied in water was calculated from the steady state average concentration of solute, c_{out}, in the outlet stream (refrigerated to

room temperature), as $c^* = (1 + Q_1/Q)c_{out}$, where Q and Q_1 were the measured volumetric flowrates.

The spheres of solutes studied were prepared from *p.a.* grade material, which was molten and then poured into moulds made of silicone rubber. Wherever any slight imperfections showed on the surface of the spheres, they were easily removed by rubbing with fine sand paper. Using callipers three measurements were made of the diameter of each sphere along three perpendicular directions.

6.4 Measurement of Tortuosity in Porous Media

The two major properties to describing porous media and the associated mass transfer phenomena are the permeability coefficient (flow phenomena) and the effective diffusion (mass transfer phenomena). However, both coefficients are functions of the characteristics of porous media, namely the media porosity and tortuosity (see [17, 18]).

The tortuosity of a packed bed is an important parameter that describes pore connectivity and fluid transport, however, it is difficult to determine experimentally. Normally, tortuosity is calculated through measured values of the porosity and the experimentally determined effective diffusion coefficient. However, tortuosity varied with the particle volume fraction and the particle size ratio in the mixture.

In recent years, nuclear magnetic resonance (NMR) has been used to determine both diffusion and tortuosity coefficients (see *e.g.* [22, 36]), with significant advantages, but it's a very expensive method.

The experiment proposed is simple and inexpensive, and it provides an accurate method for the measurement of the tortuosity in packed beds.

Tortuosity can be defined as the ratio of the distance actually travelled by a tracer through the pore space, L_e, to the straight-line distance between the two points, L, of the porous media with solute concentrations C_1 and C_2. When ignoring that the "real" length (or effective) of diffusion trajectory is sinuous the representative equation of the diffusion law it should be written as:

$$Q = D'_m \varepsilon A \frac{C_1 - C_2}{L} \tag{6.45}$$

where D'_m is the "effective" molecular diffusion coefficient. However, the applicability of Ficks first law to the "real" length of diffusion in a packed bed, L_e, result as

$$Q = D_m \varepsilon A \frac{C_1 - C_2}{L_e} \tag{6.46}$$

where D_m is the molecular diffusion coefficient. Now, by substituting Eq. 6.45 into 6.46 the following relation is obtained:

$$D'_{\mathrm{m}} = \frac{D_{\mathrm{m}}}{L_{\mathrm{e}}/L} \tag{6.47}$$

The ratio L_{e}/L being the tortuosity factor and it is usually represented by τ [7, 18]. In this work an original method for measurement of tortuosity in packed beds is presented.

Consider a vertical column containing a packed bed of inert particles, and filled with liquid to some level above the top of the packed bed (liquid "pool"). If a concentrated salt solution is then poured into this liquid "pool", with uniform concentration C_{p0}, the tracer will gradually penetrate down the packed bed. The concentration of tracer in the liquid "pool" decrease gradually in the time, until a uniform concentration of tracer, equilibrium, is reached in the whole liquid.

Analysis of the process of salt diffusion may be made in analogy with the process of diffusion from a stirred solution of limited volume, described by Crank [13]. The concentration of the dissolver salt in the packed bed, C, will vary according to (Fick's Second Law)

$$\frac{\partial C}{\partial t} = D'_{\mathrm{m}} \frac{\partial^2 C}{\partial x^2} \tag{6.48}$$

subject to the following initial and boundary conditions,

$$t = 0 \quad 0 \le x \le L \quad C = 0 \tag{6.49a}$$

$$t > 0 \quad x = 0 \quad \frac{\partial C}{\partial x} = 0 \tag{6.49b}$$

$$t > 0 \quad x = L \quad -D'_{\mathrm{m}} \varepsilon \frac{\partial C}{\partial x} = \frac{V_{\mathrm{p}}}{A} \frac{\partial C_{\mathrm{p}}}{\partial t} \tag{6.49c}$$

where V_{p} is the volume of liquid in the "pool", above the bed of inerts and A is the cross section area of the packed bed.

The solution of Eq. 6.48 with the boundary conditions (6.49a–c) could be obtained through the use of Fourier transform. However, the solution given by Crank [13] is conveniently expressed as the ratio between the amount of tracer in the bed of inert particles at any time, $\mathrm{M_t}$, and the corresponding amount of tracer after a sufficiently long time, equilibrium, M_∞ :

$$\frac{\mathrm{M_t}}{\mathrm{M}_\infty} = 1 - \sum_{\mathrm{n}=0}^{\infty} \frac{2\alpha(1+\alpha)}{1 + \alpha + \alpha^2 q_{\mathrm{n}}^2} \exp\left(-\frac{D'_{\mathrm{m}} q_{\mathrm{n}}^2 t}{L^2}\right) \tag{6.50}$$

where α is the ratio between the volume in the "pool" and the volume in the packed bed ($\alpha = V_{\mathrm{p}}/V$) and q_{n} are the non-zero positive roots of

$$\tan(q_{\mathrm{n}}) = -\alpha\, q_{\mathrm{n}} \tag{6.51}$$

As smaller is the value of $D'_m t/L^2$ more terms in the series, in Eq. 6.50, are needed for a given accuracy. When more than three or four terms are need it is better to use an alternative form of solution. For most values of α, the simplest expression is

$$\frac{M_t}{M_\infty} = (1+\alpha)\left[1 - \exp\left(\frac{D'_m t}{L^2\alpha^2}\right) \times \text{erfc}\left(\frac{D'_m t}{L^2\alpha^2}\right)^{0.5}\right] \tag{6.52}$$

The amount of tracer in the packed bed, at any time t, could be expressed by the following equation,

$$M_t = V_p\left(C_{p0} - C_p(t)\right) \tag{6.53}$$

where C_{p0} is the initial tracer concentration in the "pool"; and the equilibrium amount of tracer in the packed bed of inerts is given by

$$M_\infty = V(C_\infty - C_0) = V_p\left(C_{p0} - C_{p\infty}\right) \tag{6.54}$$

where C_0 is the initial concentration of tracer in the bed of inerts ($C_0 = 0$) and C_∞ and $C_{p\infty}$ are the equilibrium salt (tracer) concentration ($t = \infty$), in the packed bed and in the liquid "pool", respectively ($C_\infty = C_{p\infty}$). So, the equilibrium tracer concentration in packed bed could be determined as,

$$C_\infty = \frac{C_0 V + C_{p0} V_p}{V_p + V} \approx \frac{C_{p0} V_p}{V_p + V} \tag{6.55}$$

and, for experimental data, the expression of the ratio between the amount of tracer at any time t and the amount of tracer in equilibrium is given by:

$$\frac{M_t}{M_\infty} = \frac{\left(V_p + V\right)\left(C_{p0} - C_p\right)}{V\left(C_{p0} - C_0\right)} \approx \frac{\left(V_p + V\right)\left(C_{p0} - C_p\right)}{V C_{p0}} \tag{6.56}$$

In each experiment the value of α is constant and the values of C_p was measured at different times in order to determine the corresponding values of M_t/M_∞, from the appropriate representation of Eq. 6.52 or 6.54; and the value of $D'_m t/L^2$ corresponding to each value of M_t/M_∞ could be determined. For each experimental data point a plot of $D'_m t/L^2$ *vs.* t, was organized and the best straight line through the points and the origin determined. The plot gives a straight line with slope of $D'_m t/L^2$ and intercept of origin, to yield the experimental value of effective molecular diffusion coefficient, D'_m. Finally, the value of tortuosity was obtained by $\tau = D_m/D'_m$.

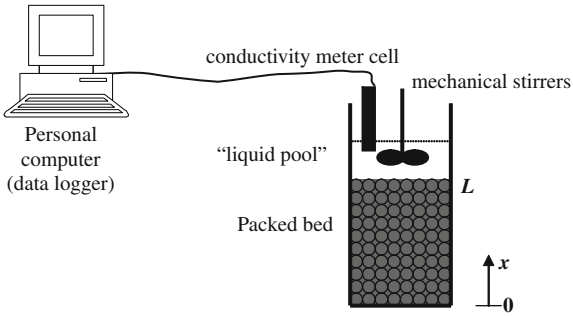

Fig. 6.11 Sketch of experimental set-up

6.4.1 Experimental Example

All measurements of tortuosity were performed in a transparent acrylic column, 0.10 m in diameter, was kept at a constant temperature using a thermostatically controlled water-bath (see Fig. 6.11).

The packed beds used in our experiments were beds of silica sand with average diameter of 0.496, 0.297, 0.219 and 0.110 mm. The silica sand was washed, dried and sieved in closely sized batches, for the experiments.

The dried silica sand was placed back inside the acrylic column at L length, and the packed bed was carefully compacted. Afterwards, distilled water, with volume V, was flowed in the "open space" of the packed bed; and a dilute salt solution flowed carefully on top of the packed bed, with volume V_p (liquid "pool"). A mechanical stirrer was used to homogenize the salt concentration in liquid "pool", with very slow rotation to avoid dispersion by forced convection.

The liquids used in the experiments were both distilled water and a dilute solution of NaCl in distilled water with a concentration of salt in the range of 0.05–2.0 M. The use of very dilute salt solutions and the care taken in equalizing the temperature of both liquids is needed to avoid dispersion by natural convection.

For each experiment the fraction of liquid volume in the packed bed, λ, was determined. The value of $\alpha = V_p/V$ used in the experiments is largely a matter of personal choice. The data in the present work refer to $\alpha \approx 1.5$.

To prevent evaporation the column are closed with a rubber cap. However, it is impossible to prevent some evaporation during the long execution time of the test.

The change of concentration in liquid "pool" was measured by monitoring decreases in the electrical conductance as a function of time. The output of this conductivity meter was connected to a micro-computer and care was taken to calibrate the conductivity cell.

6.5 Mass Transfer Around Active Solids

There are several situations of practical interest, both in nature and in man made processes, in which there is fluid flow through a bed of inert particles, packed around a solid mass that contacts with the moving fluid. Examples may be found in diverse fields, such as dilute catalyst fixed bed reactors, fluidised bed combustion, ore leaching and water contamination by buried waste. In such processes there is an interplay between diffusion, convection and dispersion and a detailed systematic study of the problem has been given by Coelho and Guedes de Carvalho [12] for transfer from buried flat surfaces and for transfer from buried spheres. Both these references present accurate solutions for certain limiting situations, namely those of low and high fluid velocity (more precisely, low and high Peclet numbers).

When the mass transfer process occur in a porous media with a fluid flowing around the soluble particle, and at low fluid velocities (as typically observed in underground flow), the assumption of thin boundary layer is not legitimate, and the theoretical analysis developed by Coelho and Guedes de Carvalho [12] is not applicable. Therefore, it is necessary to employ numerical methods for a correct analysis of the mass transfer process in more general situations.

Flow around a buried sphere is an important model situation in many processes and in a recent work Carvalho et al. [11] treated the problem numerically, so as to cover the entire range of values of Peclet and Schmidt numbers.

Flow along buried cylindrical surfaces and flat surfaces are also important model situations, and were investigated theoretically and numerically by Alves et al. [3], yielding results for a wide range of values of Peclet number, aspect ratio of soluble solid mass and Schmidt number.

Over the last years, our focus has been driven preferentially to the analysis of the mass transfer of particles with spherical geometry. This work is a contribution for the study of mass transfer of soluble particles with different geometries buried in inert particles with smaller diameter. Additionally, a simple approximate method is presented to obtain concentration contours plots for solute distribution around and downstream of the buried surfaces (with different geometries).

The following sections present a detailed description of the mass transfer and dispersion process around a soluble solid particle with different shapes (sphere, cylinder or a plane surface aligned with the flow, cylinder in cross-flow, prolate spheroid and a oblate spheroid) buried in a packed bed of smaller inert particles with uniform voidage, with a moving fluid with constant interstitial velocity.

6.5.1 Mass Transfer From a Soluble Flat Slab

Figure 6.12 sketches a section through a packed bed along which liquid is flowing, close to a flat wall, part of which ($0 < z < L$) is soluble. Liquid flow is assumed

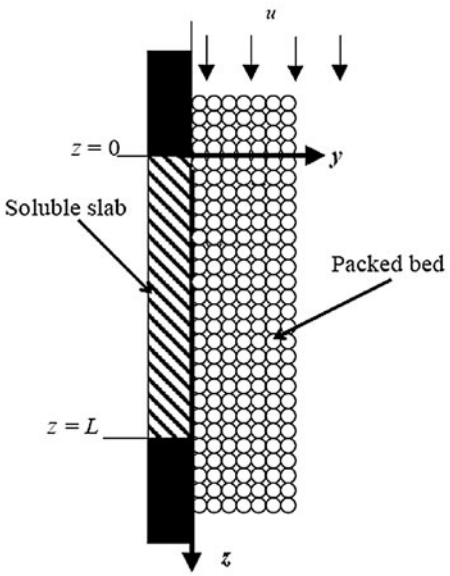

Fig. 6.12 Flow through packed bed near soluble flat surface

steady, with uniform average interstitial velocity u. If the concentration of solute in the liquid fed to the bed is c_0 and the solubility of the solid wall is c^*, a mass transfer boundary layer will develop, across which the solute concentration drops from $c = c^*$, at $y = 0$, to $c \to c_0$ for large y.

If we restrict the analysis to those situations for which the mass transfer boundary layer extends over several particle diameters and if a small control volume is considered, inside this boundary layer, with side lengths δz, δy and unity, a steady state material balance on the solute leads to

$$u\frac{\partial c}{\partial z} = D'_{\mathrm{m}}\frac{\partial^2 c}{\partial y^2} + D'_{\mathrm{m}}\frac{\partial^2 c}{\partial z^2} \tag{6.57}$$

To integrate Eq. 6.57 it is convenient to define the following dimensionless variables:

$$C = \frac{c - c_0}{c^* - c_0} \tag{6.58a}$$

$$Y = \frac{y}{L} \tag{6.58b}$$

$$Z = \frac{z}{L} \tag{6.58c}$$

$$\mathrm{Pe}'_{\mathrm{sf}} = \frac{uL}{D'_{\mathrm{m}}} \tag{6.58d}$$

where Pe'_{sf} represents the Peclet number (based on the length, L, of the soluble slab), and D'_m is the effective molecular diffusion coefficient, defined as the ratio between the molecular diffusion coefficient and the tortuosity, τ, of the packed bed ($D'_m = D_m/\tau$).

In terms of dimensionless variables, Eq. 6.57 becomes

$$pe'_{sf}\frac{\partial C}{\partial Z} = \frac{\partial^2 C}{\partial Z^2} + \frac{\partial^2 C}{\partial Y^2} \tag{6.59}$$

and the appropriate boundary conditions are

$$C \to 0 \qquad Z \to -\infty \quad \forall Y \tag{6.60a}$$

$$C = 1 \qquad 0 \le Z \le 1 \qquad Y = 0 \tag{6.60b}$$

$$\frac{\partial C}{\partial Y} = 0 \qquad Z < 0 \vee Z > 1 \qquad Y = 0 \tag{6.60c}$$

$$C \to 0 \qquad \forall Z \qquad Y \to +\infty \tag{6.60d}$$

$$C \to 0 \qquad Z \to +\infty \qquad Y \ge 0 \tag{6.60e}$$

Equation 6.59 is to be solved numerically, subjected to the boundary conditions (6.60a–6.60e), over the ranges of Pe'_{sf} of practical interest.

6.5.1.1 Discretisation

Equation 6.59 was solved numerically, using a finite-difference method in a non-uniform grid similar to that adopted by Carvalho et al. [11]. A second-order central differencing scheme was adopted for the discretisation of the diffusive terms on the right hand side of Eq. 6.59, and the convective term, on the left hand side of Eq. 6.59, was discretised using the CUBISTA high-resolution scheme of Alves et al. [3], which preserves boundedness, even for highly advective flows.

The discretised equation resulting from the finite-difference approximation of Eq. 6.59 reads:

$$pe'_{sf}\frac{C_{i+1/2,j} - C_{i-1/2,j}}{(\Delta Z_i + \Delta Z_{i+1})/2} = \frac{C_{i+1,j}(\Delta Z_i) - C_{i,j}(\Delta Z_i + \Delta Z_{i+1}) + C_{i-1,j}(\Delta Z_{i+1})}{\Delta Z_i\,\Delta Z_{i+1}(\Delta Z_i + \Delta Z_{i+1})/2} + \frac{C_{i,j+1}(\Delta Y_j) - C_{i,j}(\Delta Y_j + \Delta Y_{j+1}) + C_{i,j-1}(\Delta Y_{j+1})}{\Delta Y_j\,\Delta Y_{j+1}(\Delta Y_j + \Delta Y_{j+1})/2} \tag{6.61}$$

The $C_{i+1/2,j}$ and $C_{i-1/2,j}$ values are interpolated from the known grid node values using the CUBISTA high-resolution scheme (HRS), in order to ensure numerical stability and good precision. The normalised variable approach (NVA)

of Leonard [34] was adopted for implementations of the HRS, in which a general differencing scheme up to third order of accuracy can be expressed as

$$C_{i+1/2,j} = f(C_{i-1,j}, C_{i,j}, C_{i+1,j}) \tag{6.62}$$

The NVA uses an appropriate upwind biased normalisation, and Eq. 6.62 can be rewritten in compact form as

$$\widehat{C}_{i+1/2,j} = f(\widehat{C}_{i,j}) \tag{6.63}$$

where

$$\widehat{C}_{k,j} = \frac{C_{k,j} - C_{i-1,j}}{C_{i+1,j} - C_{i-1,j}} \quad (\text{for } k = i-1,\ i,\ i+1/2,\ i+1) \tag{6.64}$$

since, by definition of Eq. 6.64, $\widehat{C}_{i-1,j} = 0$ and $\widehat{C}_{i+1,j} = 1$.

The CUBISTA scheme is represented in the context of the NVA by the following piecewise linear functions [3]:

$$\widehat{C}_{i+1/2,j} = \begin{cases} \frac{7}{4}\widehat{C}_{i,j} & 0 \le \widehat{C}_{i,j} < \frac{3}{8} \\ \frac{3}{4}\widehat{C}_{i,j} + \frac{3}{8} & \frac{3}{8} \le \widehat{C}_{i,j} \le \frac{3}{4} \\ \frac{1}{4}\widehat{C}_{i,j} + \frac{3}{4} & \frac{3}{4} < \widehat{C}_{i,j} \le 1 \\ \widehat{C}_{i,j} & \text{elsewhere} \end{cases} \tag{6.65}$$

The resulting system of equations was solved iteratively using the successive over-relaxation (SOR) method [20], and the implementation of the boundary conditions was carried out in the same way as described in our previous work [11]. For the situation under study an orthogonal mesh is adequate and care was taken to ensure proper refinement in the regions where high concentration gradients are expected. The computational domain was defined according to the flow conditions (typically for small $\mathrm{Pe}'_{\mathrm{sf}}$, longer meshes are needed) and during mesh refinement, the number of nodes along each direction was doubled, thus halving the mesh sizes along each direction. This systematic procedure allows direct use of Richardson's extrapolation technique in order to obtain very accurate results [20].

6.5.1.2 Numerical Results

The numerical solution of Eq. 6.59 gives the concentration field and from it, the rate of dissolution of the slab, n, is obtained integrating the diffusion/dispersion flux over the whole slab surface. This integral is evaluated numerically, for each

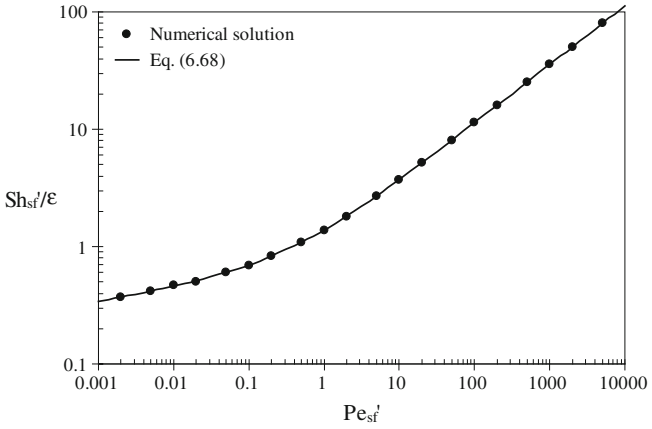

Fig. 6.13 Dependence of $\mathrm{Sh}'_{\mathrm{sf}}/\varepsilon$ on $\mathrm{Pe}'_{\mathrm{sf}}$ when $D_{\mathrm{T}} = D_{\mathrm{L}} = D'_{\mathrm{m}}$ throughout, for slab flat

set of conditions, from the discretised concentration field that is obtained through the numerical solution of Eq. 6.59. It is convenient to express the rate of dissolution in terms of a Sherwood number, $\mathrm{Sh}'_{\mathrm{sf}} = kL/D'_{\mathrm{m}}$, where $k = n/[S(c^* - c_0)]$ is the mass transfer coefficient for the soluble slab and A is the exposed area of the soluble solid.

In the analysis of the results of the numerical computations we only consider the situation of low $\mathrm{Pe}'_{\mathrm{p}}(= ud/D'_{\mathrm{m}})$ values, diffusional regime.

For low $\mathrm{Pe}'_{\mathrm{p}}$ values, dispersion is the direct result of molecular diffusion and $D_{\mathrm{T}} \cong D_{\mathrm{L}} \cong D'_{\mathrm{m}}$. Fig. 6.13 presents the results obtained numerically, for the situation of dispersion dominated by molecular diffusion, and two asymptotes can be observed:

$$\frac{\mathrm{Sh}'_{\mathrm{sf}}}{\varepsilon} \to \left(\frac{2}{\pi}\right)^{1/2} \left(\mathrm{Pe}'_{\mathrm{sf}}\right)^{1/8} \text{ for } \mathrm{Pe}'_{\mathrm{sf}} \to 0 \tag{6.66}$$

and

$$\frac{\mathrm{Sh}'_{\mathrm{sf}}}{\varepsilon} \to \left(\frac{4}{\pi}\right)^{1/2} \left(\mathrm{Pe}'_{\mathrm{sf}}\right)^{1/2} \qquad \text{for } \mathrm{Pe}'_{\mathrm{sf}} \to \infty \tag{6.67}$$

Taking the geometric mean of those two asymptotes

$$\frac{\mathrm{Sh}'_{\mathrm{sf}}}{\varepsilon} = \left[\frac{2}{\pi}\mathrm{Pe}'^{1/4}_{\mathrm{sf}} + \frac{4}{\pi}\mathrm{Pe}'_{\mathrm{sf}}\right]^{1/2} \tag{6.68}$$

one observes that it does not deviate more than 3% from the numerical values.

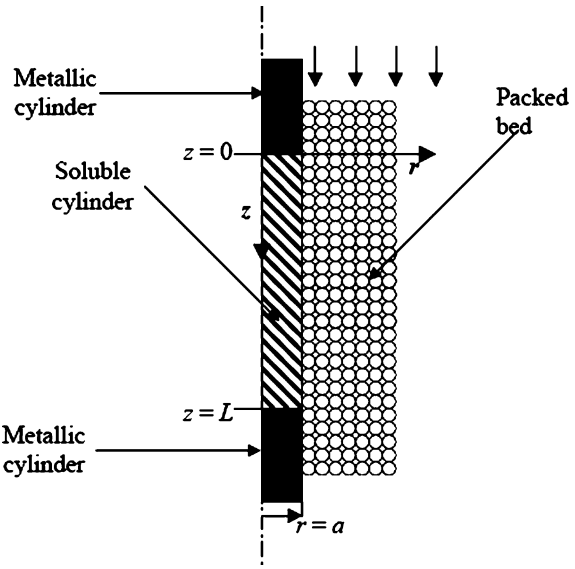

Fig. 6.14 Flow through packed bed near soluble cylinder aligned with flow

6.5.2 Mass Transfer From a Soluble a Cylinder Aligned With Flow

Figure 6.14 sketches a dissolving cylinder in a packed bed, aligned with the flow direction. In this case the mass transfer boundary layer forms around the cylinder and has axial symmetry.

Considering a small control-volume inside the boundary layer and performing a steady-state material balance on the solute, one obtains

$$\mathrm{Pe}'_{\mathrm{c}}\frac{\partial C}{\partial Z}=\frac{\partial^2 C}{\partial Z^2}+4\left(\frac{L}{d_1}\right)^2\frac{1}{R}\frac{\partial}{\partial R}\left(R\frac{\partial \mathrm{C}}{\partial R}\right) \tag{6.69}$$

where $R = 2r/d_{\mathrm{c}}$, and d_{c} represents the diameter of the soluble cylinder. Equation 6.62 was solved numerically with boundary conditions

$$\mathrm{C}\rightarrow 0 \qquad \mathrm{Z}\rightarrow -\infty \qquad \mathrm{R}\geq 1 \tag{6.70a}$$

$$\mathrm{C}=1 \qquad 0\leq \mathrm{Z}\leq 1 \qquad \mathrm{R}=1 \tag{6.70b}$$

$$\frac{\partial \mathrm{C}}{\partial \mathrm{R}}=0 \qquad \mathrm{Z}<0\vee \mathrm{Z}>1 \qquad \mathrm{R}=1 \tag{670c}$$

$$\mathrm{C}\rightarrow 0 \qquad \forall \mathrm{Z} \qquad \mathrm{R}\rightarrow +\infty \tag{6.70d}$$

$$\mathrm{C}\rightarrow 0 \qquad \mathrm{Z}\rightarrow +\infty \qquad \mathrm{R}\geq 1 \tag{6.70e}$$

over the ranges of $\mathrm{Pe}'_{\mathrm{c}}(=uL/D'_{\mathrm{m}})$ and L/d_{c} of practical interest.

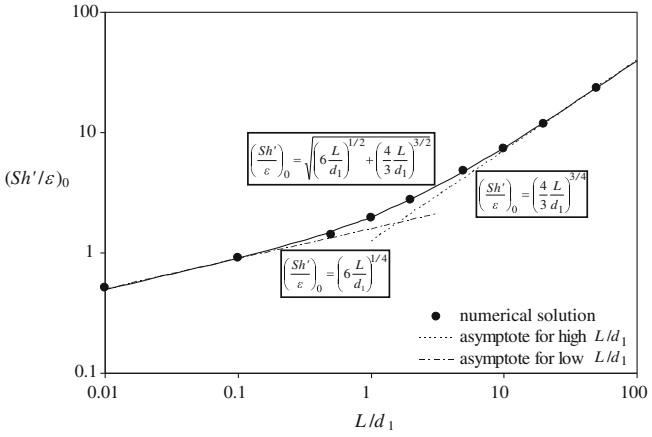

Fig. 6.15 Dependence of $(Sh'/\varepsilon)_0$ on L/d_1

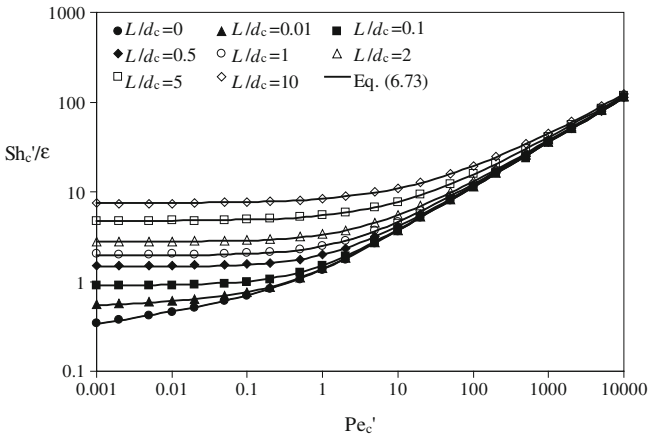

Fig. 6.16 Dependence of Sh_c'/ε on Pe_c' for different values of L/d_c

6.5.2.1 Numerical Results

For low Pe_p' values (say, $Pe_p' < 0.1$), the values of $Sh_c'/\varepsilon \left(= kL/D_m'\varepsilon\right)$ were obtained by integrating the flux along the soluble surface, in a similar way to that described for the flat surface. The first point to be mentioned is that the lower set of points in Fig. 6.16 (those for $L/d_c = 0$) were not obtained by solving Eq. 6.69 directly. Indeed, for $L/d_c \to 0$ (with finite L) the physical situation depicted in Fig. 6.15 degenerates into mass transfer from a flat surface. The plot for $L/d_c = 0$ reveals the two asymptotes obtained for the dissolution of a slab in a packed bed (see Eqs. 6.66 and 6.67. Equation 6.67 is the result obtained by Coelho and Guedes de

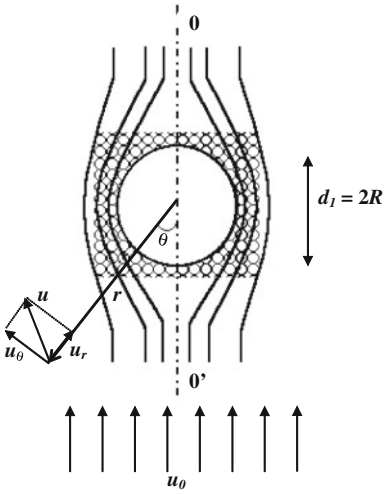

Fig. 6.17 Flow through packed bed near soluble sphere

Carvalho [12] who argued that it would be also the asymptote for $L/d_c > 0$. This is shown to be the case in Fig. 6.16 and it is not surprising, since for thin concentration boundary layer, the curvature of the cylinder is not relevant.

For each value of $L/d_c > 0$, the plot of $\mathrm{Sh}'_c/\varepsilon$ *vs.* Pe'_c has a horizontal asymptote, for $\mathrm{Pe}'_c \to 0$. This limiting value of $\mathrm{Sh}'_c/\varepsilon$ (for each value of L/d_c) may be conveniently represented by $\left(\mathrm{Sh}'_c/\varepsilon\right)_0$. to emphasize that it corresponds to the situation of pure molecular diffusion with no flow. The numerical results indicated a dependence of $\left(\mathrm{Sh}'_c/\varepsilon\right)_0$ on L/d_c and again, two asymptotes are revealed:

$$\left(\frac{\mathrm{Sh}'_c}{\varepsilon}\right)_0 \to \left(6\frac{L}{d_c}\right)^{1/4} \text{for low } \frac{L}{d_c} \tag{6.71}$$

and

$$\left(\frac{\mathrm{Sh}'_c}{\varepsilon}\right)_0 \to \left(\frac{4}{3}\frac{L}{d_c}\right)^{3/4} \text{for high } \frac{L}{d_c} \tag{6.72}$$

Having disclosed the above asymptotes, a general approximate expression for $\mathrm{Sh}'_c/\varepsilon$, that has the correct asymptotic behaviour, was found to be [4]

$$\frac{\mathrm{sh}'_c}{\varepsilon} = \left[\begin{array}{c} \frac{2}{\pi}\mathrm{pe}'_c{}^{1/4} + \frac{4}{\pi}\mathrm{pe}'_c + \left(6\frac{L}{d_c}\right)^{1/2} + \left(\frac{4}{3}\frac{L}{d_c}\right)^{3/2} \\ + \frac{5}{3}\mathrm{pe}'_c{}^{5/9}\left(\frac{L}{d_c}\right) - \mathrm{pe}'_c{}^{2/9}\left(2\frac{L}{d_c}\right)^{1/3} \end{array}\right]^{1/2} \tag{6.73}$$

This equation does not deviate more than 2% from the numerical values, over the entire range of values of Pe'_c and $L/d_c x$ represented in Fig. 6.16. The approximate conditions of validity of these equation are: $d_c/d \geq 50$ and $L/d_c \leq 100$.

6.5.3 Mass Transfer From a Soluble Sphere

Consider a soluble sphere of diameter $d_1 (d_1 = 2a)$, buried in a bed of inert particles of diameter d (with $d \ll d_1$), packed uniformly (void fraction ε) around the sphere (see Fig. 6.17). The packed bed is assumed to be "infinite" in extent and a uniform interstitial velocity of liquid, u_0, is imposed, at a large distance from the sphere.

Darcy's law, $\boldsymbol{u} = -K\,\boldsymbol{grad}\,p$, is assumed to hold and if it is coupled with the continuity relation for an incompressible fluid, $\mathrm{div}\,\boldsymbol{u} = 0$, Laplace's equation $\nabla^2\phi = 0$ is obtained for the flow potential, $\phi = K\,p$, around the sphere. In terms of spherical coordinates (r, θ), the potential and stream functions are, respectively [14],

$$\frac{\partial c}{\partial \phi} = \frac{\partial}{\partial \phi}\left(D'_m \frac{\partial c}{\partial \phi}\right) + \frac{\partial}{\partial \psi}\left(D'_m \omega^2 \frac{\partial c}{\partial \psi}\right) \tag{6.74}$$

where ω is the distance to the flow axis $(= r \sin\theta)$.

To integrate Eq. 6.74, with the auxiliary Eqs. 6.75 and 6.76, it is convenient to define the following dimensionless variables:

$$\phi = -u_0\left[1 + \frac{1}{2}\left(\frac{a}{r}\right)^3\right] r\,\cos\theta \tag{6.75}$$

$$\psi = \frac{u_0}{2}\left[1 - \left(\frac{a}{r}\right)^3\right] r^2 \sin^2\theta \tag{6.76}$$

and the velocity components are

$$u_r = \frac{\partial \phi}{\partial r} = -u_0 \cos\theta\left[1 - \left(\frac{a}{r}\right)^3\right] \tag{6.77}$$

$$u_\theta = \frac{1}{r}\frac{\partial \phi}{\partial \theta} = u_0 \sin\theta\left[1 + \frac{1}{2}\left(\frac{a}{r}\right)^3\right] \tag{6.78}$$

The analysis of mass transfer is based on a steady state material balance on the solute crossing the borders of an elementary volume, limited by the potential surfaces ϕ and $\phi + \delta\phi$, and the stream surfaces ψ and $\psi + \delta\psi$. The resulting equation is [4],

$$C = \frac{c - c_0}{c^* - c_0} \tag{6.79a}$$

$$\Re = \frac{r}{a} \tag{6.79b}$$

$$U = \frac{u}{u_0} = \frac{\left(u_r^2 + u_\theta^2\right)^{1/2}}{u_0} \tag{6.79c}$$

$$\Phi = \frac{4}{3}\frac{\phi}{u_0 d_1} \tag{6.79d}$$

$$\Psi = \frac{\psi}{u_0 d_1^2} \tag{6.79e}$$

Equation 6.78 may be re-arranged to

$$\frac{\partial C}{\partial \Phi} = \frac{\partial}{\partial \Phi}\left(\frac{4}{3\mathrm{Pe}_s'}\frac{\partial C}{\partial \Phi}\right) + \frac{\partial}{\partial \psi}\left(\frac{3}{16}\frac{\Re^2 \sin^2\theta}{\mathrm{Pe}_s'}\frac{\partial C}{\partial \psi}\right) \tag{6.80}$$

The boundary conditions to be observed in the integration of Eq. 6.74 are: (1) the solute concentration is equal to the background concentration, c_0, far away from the sphere; (2) the solute concentration is equal to the equilibrium concentration, $c = c^*$, on the surface of the sphere and (3) the concentration field is symmetric about the flow axis:

$$\Phi \to -\infty,\ \Psi \geq 0 \quad C \to 0 \tag{6.81a}$$

$$\Phi \to +\infty,\ \Psi \geq 0 \quad C \to 0 \tag{6.81b}$$

$$\Psi = 0 \begin{cases} -1 \leq \phi \leq 1 & C = 1 \\ |\phi| > 1 & \dfrac{\partial C}{\partial \Psi} = 0 \end{cases} \tag{6.81c, d}$$

$$\Psi \to +\infty,\ \text{all } \Phi \quad C \to 0 \tag{6.81e}$$

Equation 6.80 was solved numerically, subjected to the boundary conditions (6.81a–e), over the ranges of $\mathrm{Pe}_s'(= u_0 d_1 / D_m')$ of practical interest.

6.5.3.1 Numerical Results

For low values of Pe_p', dispersion is the direct result of molecular diffusion and the numerical solution obtained by Guedes de Carvalho and Alves [23] applies. Those authors showed that the numerical results are well described (with an error of less than 1% in $\mathrm{Sh}_s' = k d_1 / D_m'$) by (see Fig. 6.18)

$$\frac{\mathrm{Sh}_s'}{\varepsilon} = \left[4 + \frac{4}{5}\left(\mathrm{Pe}_s'\right)^{2/3} + \frac{4}{\pi}\mathrm{pe}_s'\right]^{1/2} \tag{6.82}$$

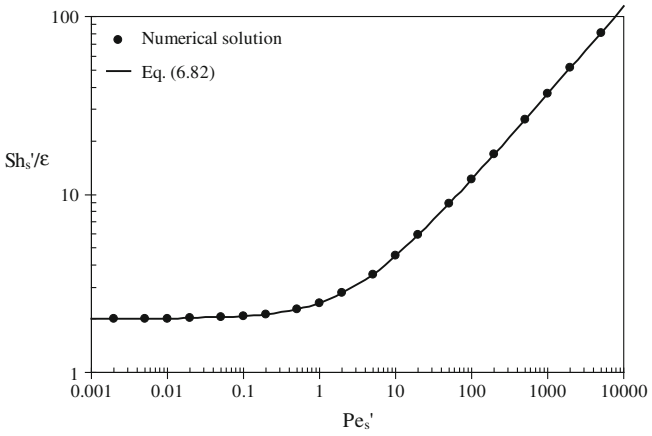

Fig. 6.18 Dependence of $\mathrm{Sh}'_s/\varepsilon$ on Pe'_s for soluble sphere

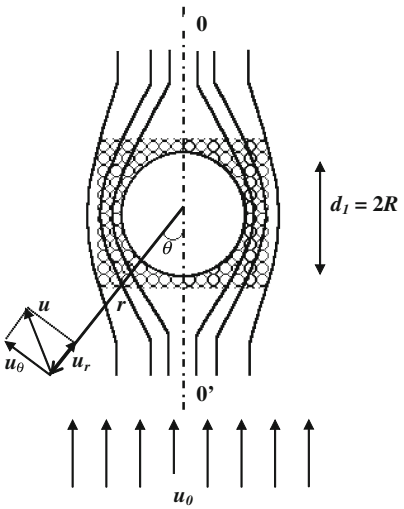

Fig. 6.19 Flow through packed bed near soluble cylinder in cross flow

6.5.4 Mass Transfer From a Cylinder in Cross Flow

Consider a slightly soluble cylinder, of diameter d_1, buried in a packed bed of inert spherical particles of diameter d ($d \ll d_1$) and exposed to fluid flow perpendicular to its axis, with uniform interstitial velocity, u_0, at a large distance from the cylinder (see Fig. 6.19).

Assuming Darcy's law, Laplace's equation is obtained for the flow potential around the cylinder. For a sufficiently long cylinder (assumed to be of "infinite"

length) the flow field is bi-dimensional and in polar coordinates, the potential and stream functions are expressed as

$$\phi = -u_0\left[1 + \left(\frac{a}{r}\right)^2\right] r\cos\theta \tag{6.83}$$

$$\psi = u_0\left[1 - \left(\frac{a}{r}\right)^2\right] r\sin\theta \tag{6.84}$$

and the velocity components are given by

$$u_r = \frac{\partial\phi}{\partial r} = -u_0\cos\theta\left[1 - \left(\frac{a}{r}\right)^2\right] \tag{6.85}$$

$$u_\theta = \frac{1}{r}\frac{\partial\phi}{\partial\theta} = u_0\sin\theta\left[1 + \left(\frac{a}{r}\right)^2\right] \tag{6.86}$$

To formulate the mass transfer problem we take the concentration of the diffusing species to be c^* on the surface of the cylinder and c_0 at a large distance from it, in the approaching stream. The resulting concentration field will have axial symmetry and the differential equation for mass transfer may be derived from a mass balance on the elementary volume.

The analysis of mass transfer is based on a steady state material balance on the solute crossing the borders of an elementary volume, limited by the potential surfaces ϕ and $\phi+\delta\phi$, and the stream surfaces ψ and $\psi + \delta\psi$. The material mass balance on the solute may be expressed as

$$\frac{\partial c}{\partial\phi} = \frac{\partial}{\partial\phi}\left(D'_{\mathrm{m}}\frac{\partial c}{\partial\phi}\right) + \frac{\partial}{\partial\psi}\left(D'_{\mathrm{m}}\frac{\partial c}{\partial\psi}\right) \tag{6.87}$$

The assumption of steady state is acceptable for a solid that is taken to be slightly soluble and the use of the dispersion coefficients makes sense if the boundary layer extends over several particle diameters.

To integrate Eq. 6.87, with the auxiliary Eqs. 6.83 and 6.84, it is convenient to define the dimensionless variables:

$$C = \frac{c - c_0}{c^* - c_0} \tag{6.88a}$$

$$\Re = \frac{r}{R} \tag{6.88b}$$

$$U = \frac{u}{u_0} = \frac{\left(u_r^2 + u_\theta^2\right)^{1/2}}{u_0} \tag{6.88c}$$

$$\Phi = \frac{\phi}{u_0 d_{\mathrm{c}}} \tag{6.88d}$$

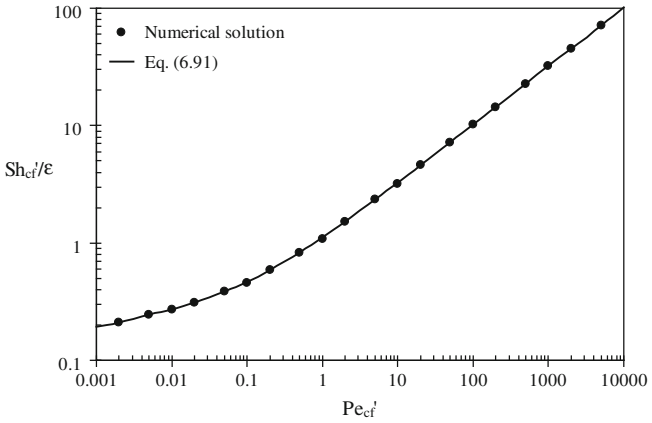

Fig. 6.20 Dependence of $\mathrm{Sh}'_{\mathrm{cf}}/\varepsilon$ on $\mathrm{Pe}'_{\mathrm{cf}}$, for a soluble cylinder in cross flow

$$\Psi = \frac{\psi}{u_0 d_\mathrm{c}} \tag{6.88e}$$

$$\mathrm{Pe}'_{\mathrm{cf}} = \frac{u_0 d_\mathrm{c}}{D'_\mathrm{m}} \tag{6.88f}$$

where $\mathrm{Pe}'_{\mathrm{cf}}$ represents the Peclet number based on the diameter of the soluble cylinder, d_c. Equation 6.87 may then be rewritten as

$$\frac{\partial C}{\partial \Phi} = \frac{\partial}{\partial \Phi}\left(\frac{1}{\mathrm{Pe}'_{\mathrm{cf}}}\frac{\partial C}{\partial \Phi}\right) + \frac{\partial}{\partial \psi}\left(\frac{1}{\mathrm{Pe}'_{\mathrm{cf}}}\frac{\partial C}{\partial \psi}\right) \tag{6.89}$$

The boundary conditions to be observed in the integration of Eq. 6.89 are: (1) the solute concentration is equal to the background concentration, c_0, far from the cylinder; (2) the solute concentration is equal to the equilibrium concentration, $c = c^*$, on the surface of the cylinder and (3) the concentration field is symmetric about $\psi = 0$.

$$\Phi \to -\infty,\ \Psi \geq 0 \quad C \to 0 \tag{6.90a}$$

$$\Phi \to +\infty,\ \Psi \geq 0 \quad C \to 0 \tag{6.90b}$$

$$\Psi = 0 \begin{cases} -1 \leq \Phi \leq 1 & C = 1 \\ |\Phi| > 1 & \dfrac{\partial C}{\partial \Psi} = 0 \end{cases} \tag{6.90c, d}$$

$$\Psi \to +\infty,\ \text{all } \Phi \quad C \to 0 \tag{6.90e}$$

Equation 6.89 has to be solved numerically and the method developed and described in detail by Alves et al. [3] was adapted, to obtain the solute concentration field around the dissolving cylinder.

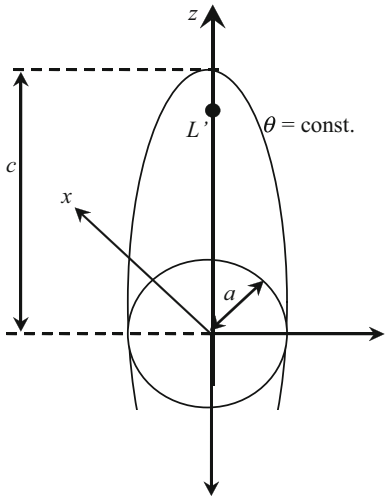

Fig. 6.21 The prolate spheroidal coordinates system

6.5.4.1 Numerical Results

For very low $\mathrm{Pe}'_{\mathrm{p}}$, dispersion is the direct result of molecular diffusion, with $D_{\mathrm{T}} \cong D_{\mathrm{L}} \cong D'_{\mathrm{m}}$, and Sherwood number is only function of Pe'. Numerical solutions were worked out for the range of Pe' between 10^{-3} and 10^{4}. The numerical values of Sh'/ε obtained are shown as dots in the plot of Fig. 6.20.

An improved approximation was found to describe the values of $\mathrm{Sh}'_{\mathrm{cf}}/\varepsilon$ obtained numerically, Eq. 6.91, which is represented as a full line in the same figure:

$$\frac{\mathrm{Sh}'_{\mathrm{cf}}}{\varepsilon} = \left[\frac{2}{\pi^2}\mathrm{Pe}'^{\,1/4}_{\mathrm{cf}} + \frac{32}{\pi^3}\mathrm{Pe}'_{\mathrm{cf}}\right]^{1/2} \tag{6.91}$$

and the values of $\mathrm{Sh}'_{\mathrm{cf}}/\varepsilon$ calculated from this equation differ at most by 2% from the corresponding numerical solution obtained in the present work.

6.5.5 Mass Transfer From a Prolate Spheroid

In many practical situations it is often required to consider operations in which there are physico-chemical interactions between a solid particle and the fluid flowing around it. In the treatment of these operations it is common practice to assume the soluble particle to be spherical, because the treatment of irregular shapes could only be done by numerical methods.

The surface of the prolate spheroid $(\theta = \theta_0)$ is described by (see Fig. 6.21)

$$\frac{x^2+y^2}{a^2}+\frac{z^2}{c^2}=1 \tag{6.92}$$

Since $r^2=x^2+y^2$, Eq. 6.92 can be written as

$$z=c\sqrt{1-(r/a)^2} \tag{6.93}$$

The surface area S and volume V of a prolate spheroid are given by

$$S=2\pi a^2\left(1+\frac{c/a}{\sqrt{1-a^2/c^2}}\sin^{-1}\left(\sqrt{1-a^2/c^2}\right)\right) \tag{6.94}$$

$$V=\frac{4}{3}\pi a^2 c \tag{6.95}$$

where $e=\sqrt{1-a^2/c^2}$ is the ellipticity, and where $e=0$ corresponds to a sphere. The dimensional Cartesian coordinates (x, y, z) are related to the prolate spheroidal ones (θ, η, β) through the equations [37]

$$x=L'\sinh\theta\sin\eta\cos\beta \tag{6.96a}$$

$$y=L'\sinh\theta\sin\eta\sin\beta \tag{6.96b}$$

$$z=L'\cosh\theta\cos\eta \tag{6.96c}$$

where L' is the focal distance $\left(L'=\sqrt{c^2-a^2}\right)$ and the coordinates range are: $0\le\theta<\infty$, $0\le\eta\le\pi$ and $0\le\beta\le2\pi$.

6.5.5.1 Analytical Results

For high Peclet numbers, with $D_T\cong D_L\cong D'_m$, our the theory is based on the assumption that the inert particles in the bed are packed with uniform voidage, ε, and that the flow may be approximated everywhere by Darcy's law, $\boldsymbol{u}=-K\,\boldsymbol{grad}\,p$. Furthermore, if the fluid is treated as incompressible, mass conservation leads to div $\boldsymbol{u}=0$, Laplace's equation is obtained $\nabla^2\phi=0$.

Darcy's law is strictly valid only for laminar flow through the packing, but according to Bear [7] it is still a good approximation for values of the Reynolds number (based on superficial velocity) up to ~10, which for beds with $\varepsilon\sim0.4$ is equivalent to $\mathrm{Re}\sim25$, the upper limit for the validity of this analysis.

When a solid prolate spheroid is immersed in a packed bed of significantly smaller particles, through which fluid flows with uniform interstitial velocity u_0, far from the spheroid, the solution of Laplace's equation and the corresponding stream function, in terms of spheroidal coordinates (θ, η, β), are [2]

$$\phi = -u_0 L' \cos\eta \left[\cosh\theta - \frac{\cosh\theta \coth^{-1}(\cosh\theta) - 1}{\coth^{-1}(\cosh\theta_0) - \dfrac{\cosh\theta_0}{\sinh^2\theta_0}} \right] \tag{6.97}$$

$$\psi = u_0 \frac{L^2}{4} \sinh\theta \left[\sinh\theta - \cos(2\eta)\sinh\theta - (1-\cos(2\eta)) \frac{\sinh\theta \coth^{-1}(\cosh\theta) - \coth\theta}{\coth^{-1}(\cosh\theta_0) - \dfrac{\cosh\theta_0}{\sinh^2\theta_0}} \right] \tag{6.98}$$

The stream and potential functions are related to the dimensionless velocity components (u_θ, u_η) by Batchelor, [5]

$$u_\theta = \frac{1}{L'\sqrt{\sinh^2\theta + \sin^2\eta}} \frac{\partial\phi}{\partial\theta} = \frac{-1}{L'^2\sqrt{\sinh^2\theta + \sin^2\eta}\sinh\theta\sin\eta} \frac{\partial\psi}{\partial\eta} \tag{6.99}$$

$$u_\eta = \frac{1}{L'\sqrt{\sinh^2\theta + \sin^2\eta}} \frac{\partial\phi}{\partial\eta} = \frac{1}{L'^2\sqrt{\sinh^2\theta + \sin^2\eta}\sinh\theta\sin\eta} \frac{\partial\psi}{\partial\theta} \tag{6.100}$$

resulting the following velocity components

$$u_\theta = \frac{-u_0\cos\eta}{\sqrt{\sinh^2\theta + \sin^2\eta}} \left[\sinh\theta - \frac{\sinh\theta \coth^{-1}(\cosh\theta) - \coth(\theta)}{\coth^{-1}(\cosh\theta_0) - \dfrac{\cosh\theta_0}{\sinh^2\theta_0}} \right] \tag{6.101}$$

$$u_\eta = \frac{u_0\sin\eta}{\sqrt{\sinh^2\theta + \sin^2\eta}} \left[\cosh\theta - \frac{\cosh\theta \coth^{-1}(\cosh\theta) - 1}{\coth^{-1}(\cosh\theta_0) - \dfrac{\cosh\theta_0}{\sinh^2\theta_0}} \right] \tag{6.102}$$

The tangential velocity at the surface of the prolate spheroid $(\theta = \theta_0)$ can be found by

$$u_{\eta 0} = \frac{1}{L'\sqrt{\sinh^2\theta + \sin^2\eta}} \left.\frac{\partial\phi}{\partial\eta}\right|_{\theta=\theta 0} \tag{6.103}$$

and the resulting expression is

$$u_{\eta 0} = \frac{u_0\sin\eta}{\left(1/e^2 - 1 + \sin^2\eta\right)^{0.5}\left[1/e - (1/e^2 - 1)\tanh^{-1} e\right]} \tag{6.104}$$

Figure 6.22 shows the adimensional tangential surface velocity, $u_{\eta 0}/u_0$, of a prolate spheroid as a function of η, for different values of the eccentricity, e. Note that, for the case of a sphere, $e \approx 0$, the well-known result of $u_{\eta 0} = 1.5u_0 \sin\eta$ is

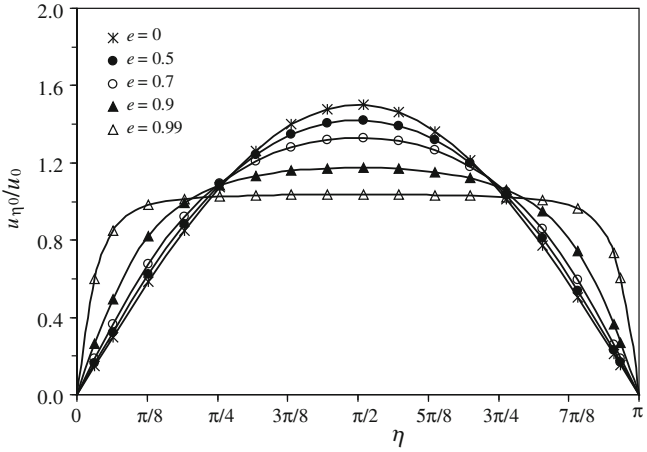

Fig. 6.22 The adimensional tangential surface velocity, $u_{\eta 0}/u_0$, as a function of η, for different values of the eccentricity, e

obtained, for potential flow over the surface of the sphere. On the other hand, for a slender prolate, $e \to 1$, as expected $u_{\eta 0}/u_0 \to 1$.

A convenient way of expressing the differential mass balance on the solute is to take a control volume along a stream tube, between two nearby potential surfaces. The resulting expression, for convection with molecular diffusion, is

$$\frac{\partial C}{\partial \phi} = \frac{\partial}{\partial \phi}\left(D'_{\mathrm{m}} \frac{\partial C}{\partial \phi}\right) + \frac{\partial}{\partial \psi}\left(D'_{\mathrm{m}} \omega^2 \frac{\partial C}{\partial \psi}\right) \tag{6.105}$$

For high values of the Peclet number the concentration boundary layer will be thin and the first term on the r.h.s. of Eq. 6.105 may be neglected. After some algebraic manipulation and a suitable change of variables, it is then possible to obtain

$$\frac{\partial \mathrm{C}}{\partial \xi} = \frac{\partial^2 \mathrm{C}}{\partial \psi^2} \tag{6.106}$$

where ξ is defined by

$$\xi = \int_0^{\eta} L'^3 \sinh^2 \theta_0 \sin^2 \eta' (\sinh^2 \theta_0 + \sin^2 \eta')^{0.5} u_\eta D'_{\mathrm{m}} d\eta' \tag{6.107}$$

with $\omega = L' \sinh \theta_0 \sin \eta$. The boundary conditions for Eq. 6.105, in our problem, are

$$C = C_0 \quad \xi = 0 \quad \psi > 0 \tag{6.108a}$$

$$C = C^* \quad \xi > 0 \quad \psi = 0 \tag{6.108b}$$

$$C \to C_0 \quad \xi > 0 \quad \psi \to \infty \tag{6.108c}$$

and the corresponding solution is

$$\frac{\mathrm{C} - \mathrm{C}_0}{\mathrm{C}^* - \mathrm{C}_0} = 1 - erf\left(\frac{\psi}{2\sqrt{\xi}}\right) \tag{6.109}$$

The value of ξ varies over the surface of the spheroid. Now, for potential flow u_η is given by Eq. 6.104 over the surface of the spheroid ($\theta = \theta_0$) and the integral in (6.107) is

$$\xi = u_0 D'_{\mathrm{m}} \frac{c^3 e^3 (1 - e^2)}{e - (1 - e^2)\tanh^{-1} e} \left(\frac{2}{3} - \cos\eta + \frac{1}{3}\cos^3\eta\right) \tag{6.110}$$

The flux of solute at any point on the surface of the spheroid is

$$\begin{aligned} N = -D'_{\mathrm{m}}\varepsilon\left(\frac{\partial C}{\partial b}\right) &= -\frac{D'_{\mathrm{m}}\varepsilon}{L'\sqrt{\sinh^2\theta_0 + \sin^2\eta}}\left(\frac{\partial C}{\partial \theta}\right)_{\theta=\theta 0} \\ &= -D'_{\mathrm{m}}\varepsilon\, u_\eta L' \sinh\theta_0 \sin\eta \left(\frac{\partial C}{\partial \psi}\right)_{\psi=0} \end{aligned} \tag{6.111}$$

and from (6.104) it may be shown that $(\partial C/\partial\psi)_{\psi=0} = \left(-1/\sqrt{(\pi\xi)}\right)(C^* - C_0)$. The rate of dissolution of the spheroid in the region $0 < \eta < \eta_1$ will then be

$$\begin{aligned} n(\eta_1) &= \int_0^{\eta 1} N 2\pi L'^2 \sqrt{\sinh^2\theta_0 + \sin^2\eta}\, \sinh\theta_0 \sin\eta \,\mathrm{d}\,\eta \\ &= \int_0^{\xi} 2\pi\varepsilon(C^* - C_0)\,(1/\sqrt{\pi z})dz = 4\sqrt{\pi}\,\varepsilon\,\xi^{1/2}(C^* - C_0) \end{aligned} \tag{6.112}$$

with $\xi(\eta_1)$given by (6.110). In particular, the total rate of dissolution of the spheroid, n_{T}, may be obtained taking $\eta_1 = \pi$. By definition, the average mass transfer coefficient, k, is

$$k = n_{\mathrm{T}} / \left[S\,(C^* - C_0)\right] \tag{6.113}$$

the resulting expression for k (from (6.112) and (6.113)) is

$$k = \frac{4\varepsilon\sqrt{\pi}}{2\pi a^2\left(1 + \dfrac{\sqrt{1/(1-e^2)}}{e}\sin^{-1}(e)\right)} \left(\frac{4}{3}\frac{c^3(1-e^2)e^3 u_0 D'_{\mathrm{m}}}{e - (1-e^2)\tanh^{-1} e}\right)^{1/2} \tag{6.114}$$

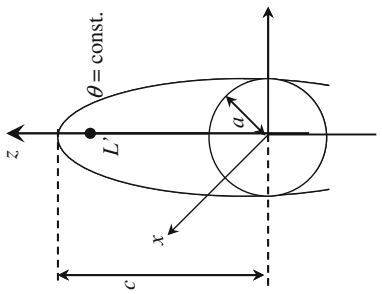

Fig. 6.23 The oblate spheroidal coordinates system

It is convenient to express the rate of dissolution in terms of the Sherwood number, $\mathrm{Sh}'_{\mathrm{ps}} = kd_{\mathrm{eq}}/D'_{\mathrm{m}}$, with $d_{\mathrm{eq}} = 2(a^2c)^{1/3}$, and the expression obtained, after some algebraic manipulation is

$$\frac{\mathrm{sh}'_{\mathrm{ps}}}{\varepsilon} = \sqrt{\frac{4}{\pi}\mathrm{Pe}'_{\mathrm{ps}}}\left(\frac{2}{3}\frac{e^3}{e-(1-e^2)\tanh^{-1}e}\right)^{1/2}\frac{2}{(1-e^2)^{1/3}+\frac{(1-e^2)^{-1/6}}{e}\sin^{-1}e} \tag{6.115}$$

where $\mathrm{Pe}'_{\mathrm{ps}} = u_0 d_{\mathrm{eq}}/D'_{\mathrm{m}}$ is the Peclet number. It is expected that Eq. 6.115 does not differ by more than 10% from the exact solution to obtain numerically.

For the special case of a sphere, $e \approx 0$, the result of $\mathrm{Sh}'_{\mathrm{s}}/\varepsilon = [4\,\mathrm{Pe}'/\pi]^{1/2}$ is obtained, which corresponds to the asymptotic behaviour for thin concentration layer (high values of Peclet number) when dispersion is constant and tend to D'_{m} over the surface of the sphere.

6.5.6 Mass Transfer From an Oblate Spheroid

The surface area S of an oblate spheroid is given by

$$S = 2\pi a^2\left(1+\frac{(c/a)^2}{2\sqrt{1-c^2/a^2}}\ln\left(\frac{1+\sqrt{1-c^2/a^2}}{1-\sqrt{1-c^2/a^2}}\right)\right) \tag{6.116}$$

where $e = \sqrt{1-c^2/a^2}$ is the ellipticity, and for $e = 0$ corresponds to a sphere. Figure 6.23 describes the oblate spheroidal coordinate system.

The dimensional Cartesian coordinates (x, y, z) are related to the oblate spheroidal ones (θ, η, β) through the equations

$$x = L'\cosh\theta\sin\eta\cos\beta \tag{6.117a}$$

$$y = L'\cosh\theta\sin\eta\sin\beta \tag{6.117b}$$

$$z = L' \sinh\theta \cos\eta \tag{6.117c}$$

where $L' = \sqrt{a^2 - c^2}$ is the focal distance and the coordinates are $0 \le \theta < \infty,\ 0 \le \eta \le \pi$ and $0 \le \beta \le 2\pi$.

6.5.6.1 Analytical Results

For high values of Peclet numbers, the theory used is based on the assumption that the inert particles in the bed are packed with uniform voidage, ε, and that the fluid flow may be approximated everywhere by Darcy's law, $\mathbf{u} = -K\,\mathbf{grad}\,p$, as in the case of a prolate spheroid.

When a solid oblate spheroid is immersed in a packed bed of significantly smaller particles, through which fluid flows with uniform interstitial velocity u_0, far from the spheroid, the solution of Laplace's equation and the corresponding stream function, in terms of spheroidal coordinates (θ, η, β), are [2]

$$\phi = -u_0 L' \cos\eta \left[\sinh\theta - \frac{\sinh\theta \cot^{-1}(\sinh\theta) - 1}{\cot^{-1}(\sinh\theta_0) - \dfrac{\sinh\theta_0}{\cosh^2\theta_0}} \right] \tag{6.118}$$

$$\psi = u_0 \frac{L^2}{4} \cosh\theta \left[\begin{array}{l} \cosh\theta - \cos(2\eta)\cosh\theta \\ -(1 - \cos(2\eta)) \dfrac{\cosh\theta \cot^{-1}(\sinh\theta) - \tanh\theta}{\cot^{-1}(\sinh\theta_0) - \dfrac{\sinh\theta_0}{\cosh^2\theta_0}} \end{array} \right] \tag{6.119}$$

The stream and potential functions are related to the dimensionless velocity components and resulting the following velocity components

$$u_\theta = \frac{-u_0 \cos\eta}{\sqrt{\cosh^2\theta - \sin^2\eta}} \left[\cosh\theta - \frac{\cosh\theta \cot^{-1}(\sinh\theta) - \tanh(\theta)}{\cot^{-1}(\sinh\theta_0) - \dfrac{\sinh\theta_0}{\cosh^2\theta_0}} \right] \tag{6.120}$$

$$u_\eta = \frac{u_0 \sin\eta}{\sqrt{\cosh^2\theta - \sin^2\eta}} \left[\sinh\theta - \frac{\sinh\theta \cot^{-1}(\sinh\theta) - 1}{\cot^{-1}(\sinh\theta_0) - \dfrac{\sinh\theta_0}{\cosh^2\theta_0}} \right] \tag{6.121}$$

The tangential velocity at the surface of the oblate spheroid ($\theta = \theta_0$) can be found by

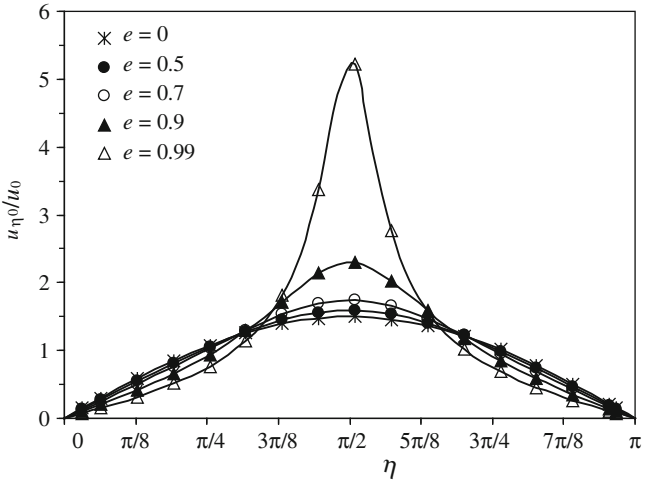

Fig. 6.24 The adimensional tangential surface velocity, $u_{\eta 0}/u_0$, as a function of η, for different values of the eccentricity, e

$$u_{\eta 0} = \frac{1}{L'\sqrt{\cosh^2\theta - \sin^2\eta}} \frac{\partial \phi}{\partial \eta}\bigg|_{\theta=\theta 0} = \frac{u_0 \sin\eta}{\left(\frac{1}{e^2} - \sin^2\eta\right)^{0.5}\left[-\sqrt{\frac{1-e^2}{e^2}} + \frac{1}{e^2}\cot^{-1}\left(\sqrt{\frac{1-e^2}{e^2}}\right)\right]} \tag{6.122}$$

Figure 6.24 shows the adimensional tangential surface velocity, $u_{\eta 0}/u_0$, of a prolate spheroid as a function of η, for different values of the eccentricity, e. Note that, for the case of a sphere, $e \approx 0$, the well-known result of $u_{\eta 0} = 1.5u_0 \sin\eta$ is obtained, for potential flow over the surface of the sphere. On the other hand, for a slender oblate, $e \to 1$, as expected $u_{\eta 0}/u_0 \to 1$.

A convenient way of expressing the differential mass balance on the solute is to take a control volume along a stream tube, between two nearby potential surfaces. The resulting expression, for convection with molecular diffusion, is given by Eq. 6.99, where ξ is defined by

$$\xi = \int_0^\eta L'^3 \cosh^2\theta_0 \sin^2\eta' (\cosh^2\theta_0 - \sin^2\eta')^{1/2} u_\eta D'_{\mathrm{m}} \, \mathrm{d}\eta' \tag{6.123}$$

with $\omega = L' \cosh\theta_0 \sin\eta$. The boundary conditions for are given by Eqs. 6.108a–c and the corresponding solution is

$$\frac{C - C_0}{C^* - C_0} = 1 - erf\left(\frac{\psi}{2\sqrt{\xi}}\right) \tag{6.124}$$

The value of ξ varies over the surface of the spheroid. Now, for potential flow u_η is given by Eq. 6.115 over the surface of the spheroid ($\theta = \theta_0$) and the integral in (6.125) is

$$\xi = u_0 D'_m \frac{e^3 c^3/(1-e^2)}{-e + e^3 + \sqrt{1-e^2}\cot^{-1}(\sqrt{1/e^2-1})}\left(\frac{2}{3} - \cos\eta + \frac{1}{3}\cos^3\eta\right) \tag{6.125}$$

The flux of solute at any point on the surface of the spheroid is

$$N = -\frac{D'_m \varepsilon}{L'\sqrt{\cosh^2\theta_0 - \sin^2\eta}} = -D'_m \varepsilon u_\eta L' \cosh\theta_0 \sin\eta \left(\frac{\partial C}{\partial \psi}\right)_{\psi=0}\left(\frac{\partial C}{\partial \theta}\right)_{\theta=\theta 0} \tag{6.126}$$

and from (6.126) it may be shown that $(\partial C/\partial\psi)_{\psi=0} = \left(-1/\sqrt{(\pi\xi)}\right)(C^* - C_0)$. The rate of dissolution of the spheroid in the region $0 < \eta < \eta_1$ will then be

$$n(\eta_1) = \int_0^{\eta 1} N 2\pi L'^2 \sqrt{\cosh^2\theta_0 - \sin^2\eta}\cosh\theta_0 \sin\eta \, d\eta = 4\sqrt{\pi}\,\varepsilon\,\xi^{1/2}(C^* - C_0) \tag{6.127}$$

with $\xi(\eta_1)$given by (6.125). In particular, the total rate of dissolution of the spheroid, n_T, may be obtained taking $\eta_1 = \pi$. By definition, the average mass transfer coefficient, k, is given by Eq. 6.106 and the resulting expression for k is

$$k = \frac{4\varepsilon\sqrt{\pi}}{2\pi a^2\left(1 + \frac{1-e^2}{2e}\ln\left(\frac{1+e}{1-e}\right)\right)}\left(\frac{2}{3}\frac{e^3 u_0 D'_m c^3/(1-e^2)}{-e + e^3 + \sqrt{1-e^2}\cot^{-1}(\sqrt{1/e^2-1})}\right)^{1/2} \tag{6.128}$$

It is convenient to express the rate of dissolution in terms of the Sherwood number, $Sh'_{os} = kd_{eq}/D'_m$, with $d_{eq} = 2(a^2 c)^{1/3}$, and the expression obtained is

$$\frac{Sh'_{os}}{\varepsilon} = \sqrt{\frac{4}{\pi}Pe'_{os}}\left(\frac{4}{3}\frac{e^3}{-e + e^3 + \sqrt{1-e^2}\cot^{-1}(\sqrt{1/e^2-1})}\right)^{1/2}\frac{(1-e^2)^{1/3}}{1 + \frac{1-e^2}{2e}\ln\left(\frac{1+e}{1-e}\right)} \tag{6.129}$$

where $Pe'_{os} = u_0 d_{eq}/D'_m$ is the Peclet number.

References

1. Akehata, T., Sato, K.: Flow distribution in packed beds. Chem. Eng. Jpn. **22**, 430–436 (1958)
2. Alassar, R.S., Badr, H.M.: Analytical solution of oscillating inviscid flow over oblate spheroids with spheres and flat disks as special cases. Ocean Eng. **24**, 217–225 (1997)
3. Alves, M.A., Oliveira, P.J., Pinho, F.T.: A convergent and universally bounded interpolation scheme for the treatment of advection. Int. J. Num. Meth. Fluids **41**, 47–75 (2003)
4. Alves, M.A., Delgado, J.M.P.Q., Guedes de Carvalho, J.R.F.: Mass transfer from cylinders and plane surfaces buried in packed beds in alignment with the flow direction. Chem. Eng. Sci. **61**, 1174–1183 (2006)
5. Batchelor, G.K.: An Introduction to Fluid Dynamics. Cambridge University Press, Cambridge (1997)
6. Baetsle, L.H.: Migration of radionuclides in porous media. In: Duhamed Pergamon, A.M.F. (ed.) Progress in Nuclear Energy, Series XII, pp. 707–730. Health Physics, Elmsford (1969)
7. Bear, J.: Dynamics of Fluids in Porous Media. Dover Publications, New York (1972)
8. Blackwell, R.J.: Laboratory studies of microscopic dispersion phenomena. Soc. Petrol. Eng. J. **225**, 1–8 (1962)
9. Bruinzeel, C, Reman, GH, van der Laan, ETh Axial dispersion. Proceedings of the 3th Congress of the European Federation of Chemical Engineering, Olympia (1962)
10. Carslaw, H.S., Jaeger, J.C.: Conduction of Heat in Solids, 2nd edn. Oxford University Press, Oxford (1959)
11. Carvalho, J.R.F.G., Delgado, J.M.P.Q., Alves, M.A.: Mass transfer between flowing fluid and sphere buried in packed bed of inerts. AIChE J. **50**, 65–74 (2004)
12. Coelho, M.A.N., Guedes de Carvalho, J.R.F.: Transverse dispersion in granular beds. Part I: Mass transfer from a wall and the dispersion coefficient in packed beds. Chem. Eng. Res. Des. **66**, 165–177 (1988)
13. Crank, J.: The Mathematics of Diffusion, 2nd edn. Oxford University Press, Oxford (1975)
14. Currie, I.G.: Fundamental Mechanics of Fluids. McGraw-Hill, New York (1993)
15. Danckwerts, P.V.: Continuous flow systems. Chem. Eng. Sci. **2**, 1–13 (1953)
16. Dorweiler, V.P., Fahien, R.W.: Mass transfer at low flow rates in a packed column. AIChE J. **5**, 139–144 (1959)
17. Dullien, F.A.L.: Single phase flow through porous media and pore structure. Chem. Eng. J. **10**, 1–34 (1975)
18. Dullien, F.A.L.: Porous Media: Fluid Transport and Pore Structure. Academic, San Diego (1979)
19. Fahien, R.W., Smith, J.M.: Mass transfer in packed beds. AIChE J. **1**, 28–37 (1955)
20. Ferziger, J.H., Peric, M.: Computational Methods for Fluid Dynamics. Springer, Berlin (1996)
21. Fuller, E.N., Schettler, P.D., Giddings, J.C.: A new method for prediction of binary gas-phase diffusion coefficients. Ind. Eng. Chem. **58**, 19–27 (1966)
22. Gibbs, S.J., Lightfoot, E.N., Root, T.W.: Protein diffusion in porous gel filtration chromatography media studied by pulsed field gradient NMR spectroscopy. J. Phys. Chem. **96**, 7458–7462 (1992)
23. Guedes de Carvalho, J.R.F., Alves, M.A.M.: Mass transfer and dispersion around active sphere buried in a packed bed. AIChE J. **45**, 2495–2502 (1999)
24. Guedes de Carvalho, J.R.F., Delgado, J.M.P.Q.: Lateral dispersion in liquid flow through packed beds at $Pe_m < 1400$. AIChE J. **46**, 1089–1095 (2000)
25. Gunn, D.J.: Mixing in packed and fluidised beds. Chem. Eng. **219**, CE153–CE172 (1968)
26. Gunn, D.J., Pryce, C.: Dispersion in packed beds. Trans. IChemE **47**, T341–T350 (1969)
27. Han, N.W., Bhakta, J., Carbonell, R.G.: Longitudinal and lateral dispersion in packed beds: effect of column length and particle size distribution. AIChE J. **31**, 277–288 (1985)
28. Harleman, D.R.F., Rumer, R.: Longitudinal and lateral dispersion in an isotropic porous medium. J. Fluid Mech. **16**, 1–12 (1963)

29. Harrison, D., Lane, M., Walne, D.J.: Axial dispersion of liquid on a column of spheres. Trans. IChemE **40**, 214–220 (1962)
30. Hiby, J.W., Schummer, P.: Zur messung der transversalen effektiven diffusion in durchstromten fullkorpersaulen. Chem. Eng. Sci. **13**, 69–74 (1960)
31. Higbie, S.: The rate of absorption of a pure gas into a still liquid during short periods of exposure. Trans. AIChE J. **31**, 365–389 (1935)
32. Hunt, B.: Dispersive sources in uniform groundwater flow. J. Hydraul. Div.–Proc. Am. Soc. Civil Eng. **104**, 75–85 (1978)
33. Klinkenberg, A., Krajenbrink, H.J., Lauwerier, H.A.: Diffusion in a fluid moving at uniform velocity in a tube. Ind. Eng. Chem. **45**, 1202–1208 (1953)
34. Leonard, B.P.: Simple high-accuracy resolution program for convective modelling of discontinuities. Int. J. Num. Meth. Fluids **8**, 1291–1318 (1988)
35. Marrero, T.R., Mason, E.A.: Gaseous diffusion coefficients. J. Phys. Chem. Ref. Data **1**, 3–25 (1972)
36. Mair, R.W., Hurlimann, M.D., Sen, P.N., Schwartz, L.M., Patz, S., Walsworth, R.L.: Tortuosity measurement and the effects of finite pulse widths on xenon gas diffusion NMR studies of porous media. Mag. Reson. Imag. **193**, 345–351 (2001)
37. Moon, P., Spencer, D.E.: Field theory handbook (2nd ed). Springer, Berlin (1971)
38. National Research Council: International critical tables–Volume 5. McGraw-Hill International Editions, New York (1929)
39. Ogata, A., Banks, R.B.: A solution of differential equation of longitudinal dispersion in porous media. US Geolog. Surv. Prof. Pap. **411-A**:7–12 (1961)
40. Perkins, T.K., Johnston, O.C.: A review of diffusion and dispersion in porous media. Soc. Petrol. Eng. J. **2**, 70–84 (1963)
41. Perry, R.H., Green, D.: Perry's chemical engineer's handbook (6th ed). McGraw-Hill International Editions, New York (1984)
42. Pinto, A.M.F.R., Guedes de Carvalho, J.R.F.: Transverse dispersion in granular beds. Part III: Mass transfer around particles dispersed in granular beds of inerts and the combustion of carbon particles in beds of sand. Trans. IChemE **68**, 503–509 (1980)
43. Plautz, D.A., Johnstone, H.F.: Heat and mass transfer in packed beds. AIChE J. **1**, 193–199 (1955)
44. Reid, R.C., Prausnitz, J.M., Poling, B.E.: The properties of gases and liquids (4th ed). McGraw-Hill International Editions, New York (1988)
45. Rifai, M.N.E., Kaufman, W.J., Todd, D.K.: Dispersion phenomena in laminar flow through porous media. University of California, Sanitary Engineering Report 3. Inst. Eng. Res. Series **90**, 1–157 (1956)
46. Robbins, G.A.: Methods for determining transverse dispersion coefficients of porous media in laboratory column experiment. Water Resour. Res. **25**, 1249–1258 (1989)
47. Roemer, G., Dranoff, J.S., Smith, J.M.: Diffusion in packed beds at low flow rates. Ind. Eng. Chem. Fund. **1**, 284–287 (1962)
48. Sherwood, T.K., Pigford, R.L., Wilke, C.R.: Mass Transfer. McGraw-Hill International Editions, Tokyo (1975)
49. Sinclair, R.J., Potter, O.E.: The dispersion of gas in flow through a bed of packed solids. Trans. IChemE **43**, T3–T9 (1965)
50. Stephenson, J.L., Stewart, W.E.: Optical measurements of porosity and fluid motion in packed beds. Chem. Eng. Sci. **41**, 2161–2170 (1986)
51. Sun, N.Z.: Mathematical modelling of groundwater pollution. Springer, New York (1996)
52. Taylor, G.: Dispersion of soluble matter in solvent flowing slowly through a tube. P. Roy Soc. A –Math. Phy. **219**, 186–203 (1953)
53. Uno, S.: Mass Transfer from naphthalene slabs. PhD Dissertation, Illinois Institute of Technology, Chicago (1958)
54. Van Genuchten, M.Th., Alves, W.J.: Analytical solutions of the one-dimensional convective-dispersive solute transport equation. Tech. Bull. U.S. Dep. Agric. **1661**, 149–165 (1982)

55. Vortmeyer, D., Schuster, J.: Evaluation of steady flow profiles in rectangular and circular packed beds by a variational method. Chem. Eng. Sci. **38**, 1691–1699 (1983)
56. Wakao, N., Funazkri, T.: Effect of fluid dispersion coefficients on particle-to-fluid mass transfer coefficients in packed beds. Chem. Eng. Sci. **33**, 1375–1384 (1978)